Available online at www.sciencedirect.com
SCIENCE DIRECT®
Journal of Computational Physics 188 (2003) 365–398
JOURNAL OF COMPUTATIONAL PHYSICS
www.elsevier.com/locate/jcp

Acoustic perturbation equations based on flow decomposition via source filtering

R. Ewert *, W. Schröder

Aerodynamisches Institut, RWTH Aachen, Wüllnerstrasse zw. 5 und 7, D-52062 Aachen, Germany

Received 25 April 2002; received in revised form 28 November 2002; accepted 12 March 2003

Abstract

A family of acoustic perturbation equations is derived for the simulation of flow-induced acoustic fields in time and space. The mean flow convection and refraction effects are part of the simulation of wave propagation. Using linearized acoustic perturbation equations the unbounded growth of hydrodynamic instabilities in critical mean flows is prevented completely. The perturbation equations are excited by source terms determined from a simulation of the compressible or the incompressible flow problem. Since the simulation of wave propagation contains the convection effects the computational domain of the flow simulation has to comprise only the significant acoustic source region. The acoustic perturbation equations are validated by computing a monopole source in a sheared mean flow, the sound generated due to a spinning vortex pair, and the sound generated by a cylinder in a crossflow.

Keywords: Acoustic perturbation equations; LES; CAA; Flow decomposition; Source filtering

1. Introduction

To simulate flow-induced noise a hybrid two step approach is considered. The first step consists of a simulation of the unsteady compressible flow problem just in the area where noise is generated. Since the fluid dynamical and acoustical length scales differ considerably for small Mach numbers, the acoustic field is computed in a second step using acoustic perturbation equations that describe the propagation of acoustic waves in time and space. Its computational domain has a substantially larger extension compared to that of the flow simulation due to the increased grid spacing allowed for the acoustic simulation. The constraints concerning the grid resolution of the unsteady flow simulation are given by the size of a typical turbulent integral length scale. The Strouhal number $St = \omega L/u$ can be interpreted to be proportional to the reciprocal value of the non-dimensional length scale of convective vortical disturbances λ_v, i.e., $St \propto (\lambda_v/L)^{-1}$. The inverse of the non-dimensional acoustic wavelength λ is defined by the Helmholtz

* Corresponding author.
E-mail address: roland.ewert@dlr.de (R. Ewert).

0021-9991/03/$ - see front matter
doi:10.1016/S0021-9991(03)00168-2

number $He = \omega L/c = StM \propto (\lambda/L)^{-1}$, where $M = u/c$ is the Mach number of the problem. Hence, vortical structures generate acoustic waves with a M^{-1} larger length scale.

Numerous noise problems in aeronautics are related to flows at Mach numbers of the order of $M \approx 10^{-1}$, e.g., airframe-noise of aircraft during take-off and landing. For such problems an acoustic domain with an extension at least one order of magnitude larger than the core domain of the flow simulation can be used with a comparable number of mesh points in the acoustic and the flow domain, respectively.

For example, consider the noise generated by the turbulent flow in the vicinity of a sharp trailing edge of an airfoil section, Fig. 1. In this problem, the unsteady turbulent compressible flow close to the trailing edge is computed in the first step using computational fluid dynamics (CFD) methods capable to resolve the essential unsteady scales, e.g., large eddy simulation (LES) or direct numerical simulation (DNS).

The second step consists of the simulation of the acoustic field by solving acoustic perturbation equations in a computational domain, which comprises apart from the CFD region the remaining geometry not resolved in the unsteady flow simulation. For the discretization of the acoustic perturbation equations numerical methods developed in the framework of computational aeroacoustics (CAA) are applied. The diffraction of acoustic waves at the leading edge and the geometry of the complete surface are taken into account as part of the acoustic simulation. Furthermore, the acoustic perturbation equations are the appropriate governing equations to describe wave propagation in the inhomogeneous acoustic domain where the mean flow field deviates considerably from the free-flow values. In this case, the homogeneous convected wave equation with constant coefficients does not describe wave propagation physically exact.

Besides the perturbation equations based on a compressible flow simulation proposed in this study several other approaches are given in the literature to determine the acoustic field in the second step of hybrid prediction methods [23], e.g.,

- acoustic analogies,
- perturbation equations based on an incompressible flow simulation.

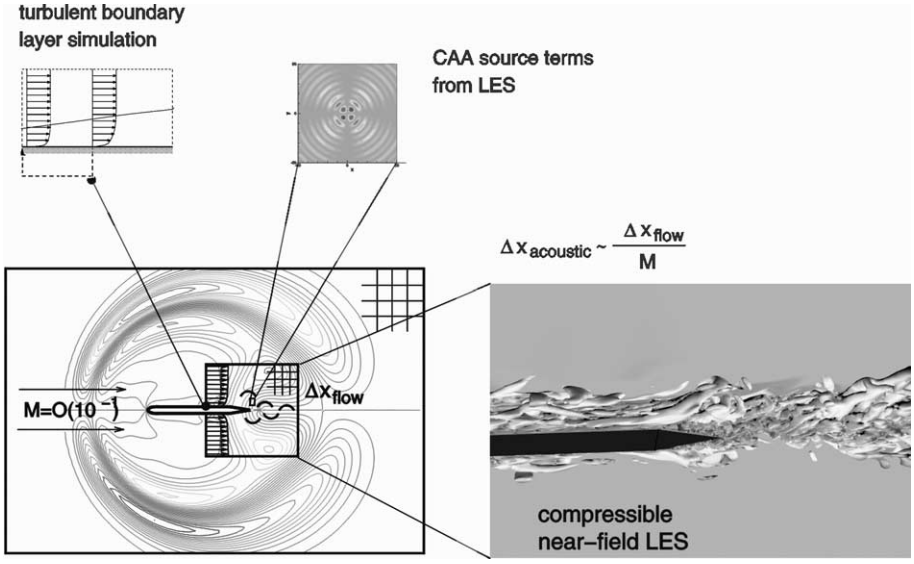

Fig. 1. Sketch of the computational domains to determine trailing edge noise with the hybrid approach. The LES domain encompasses the vicinity of the trailing edge whereas the computational aeroacoustics (CAA) domain includes the whole airfoil due to the less stringent demands concerning the grid resolution ($\Delta x_{\text{acoustic}} \sim \Delta x_{\text{LES}}/M$, $M = \mathcal{O}(10^{-1})$). Thus, scattering at the leading edge can be captured and directivities can be predicted.

The first and most famous acoustic analogy is that of Lighthill [24]. Lighthill rearranged the continuity and the Navier–Stokes equations such that the left-hand side represents an acoustic wave equation describing wave propagation in a quiescent or, via Galilean transformation, in a uniformly moving medium, which is excited by a right-hand side source. This source describes besides acoustic sources also convection and refraction effects in the inhomogeneous acoustic domain. Considering the trailing edge problem, Fig. 1, the source of Lighthill's equation has to be determined not only in the area close to the trailing edge, but also in the remaining inhomogeneous acoustic domain to take into account non-uniform convection effects, that can be large even for small Mach number flows [4]. Grogger et al. [15] showed that the convection effects due to the irrotational flow field around a 12% Zhukhovski airfoil are not sufficiently described by assuming a simple constant convection speed.

As an extension of the Lighthill equation the Ffowcs Williams–Hawkings (FW–H) equation allows to consider solid surfaces by using information of the unsteady surface pressure. For the problem in Fig. 1 the pressure distribution on the front part of the airfoil is unknown and the application of the FW–H equation in the frequency domain yields rather a system of equations for these unknowns than an explicit prediction method. Neglecting these pressure fluctuations might lead to errors of several *dBs* [26]. The wave operator of Lilley's acoustic analogy [25] describes exactly convection effects for shear flows [12]. However, as pointed out in [34], Lilley's equation includes the prediction of hydrodynamic instabilities and thus, solutions can become unstable at critical mean flow profiles.

Hybrid methods based on a decomposition of the flow field into incompressible hydrodynamics and compressible perturbation equations, e.g., the non-linear methods proposed by Hardin and coworkers [16,17,32], Shen and Sørensen [35,36], and Slimon et al. [37], in principle exclude the backscatter of acoustic perturbations onto the incompressible flow field that could be important for some acoustic source mechanisms. On the other hand, hybrid methods, which allow the use of sources based on a compressible and unsteady flow simulation for linearized perturbation equations, e.g., the linearized Euler equations (LEE) with non-linear source terms, might suffer from excited hydrodynamic instabilities. Since the linearized Euler equations describe the propagation of acoustic, vorticity, and entropy waves unstable solutions of the LEE in a globally unstable mean flow occur. This is evidenced in Section 4.4 for the mean flow field of a cylinder in a crossflow (Fig. 11).

The purpose of this work is the formulation of acoustic perturbation equations driven by sources determined from a compressible flow simulation. The various systems of acoustic equations will be shown to be hydrodynamically stable. For low Mach number problems the grid resolution can be strongly reduced since the convection modes with their smaller length scales are suppressed.

Since convection effects are described by the wave operator encoded in the acoustic perturbation equations, they are unlike the source of Lighthill's acoustic analogy excluded from the right-hand side sources. That is, the extension of the source domain, which has to be resolved in the flow simulation in the first step, can be significantly reduced, thus it is computationally less expensive. The acoustic domain is large enough to compute directivities in the near far field. If necessary, however, the results from the acoustic simulation can be used as input for Kirchhoff methods applied on the interface between the inhomogeneous and the homogeneous acoustic domain, where the mean flow is sufficiently uniform such that the homogeneous constant-coefficient wave equations describe wave propagation physically correct.

The paper is organized as follows. In Section 2, the source-term filtering is proposed which extracts from an initially time-dependent source of the linearized Euler equations only those contributions related to an acoustic source. In Section 3, the filtering technique is used to derive acoustic perturbation equations (APE), which take into account the convection and refraction effects due to a non-uniform base flow field. The wave propagation in a sheared mean flow, the spinning vortex pair, and the sound generated by a circular cylinder in laminar subsonic flow are used as test problems in Section 4 to juxtapose the solutions of the APE and other perturbation equations. Finally, the essential findings are summarized in Section 5.

2. Source filtering

A significant noise source arises from the interaction of unsteady flow fields with geometric inhomogeneities, e.g., noise originating from leading and trailing edges of a wing or fan or compressor blades. These noise sources can be understood as the transformation of the energy of vorticity waves into acoustical energy. As shown by Chu and Kovásznay [2] a compressible flow can be represented as a sum of vortical, entropy, and acoustic components. The linearized Euler equations have three eigenmodes representing these components. Therefore, these equations can be used to simulate the above-mentioned sound source mechanism, e.g., by injecting vorticity into the flow field upstream of a sound generating obstacle [5,6].

If the sound field is computed using a simulation of the unsteady compressible flow problem in the area where the noise is generated one has to be aware that the interaction of vorticity with the geometry and the generation of acoustic responses are part of the flow simulation. In general, it is possible to split the simulation of acoustic wave propagation and the computation of the acoustic sources, which arise from the unsteady flow. Such a separation of the analysis of the flow field and the acoustic field offers the possibility to take advantage of the disparity of the turbulent and acoustic scales at low Mach numbers.

We turn now to the derivation of a source term that excites purely acoustic modes. The governing fluid dynamics equations, i.e., mass, momentum, and energy equation, are rewritten such that the left-hand side corresponds to the linearized inviscid (Euler) equations plus the linearized energy and continuity equations, while the right-hand side is the source term given by the non-linear and viscous terms. In general, this source term will generate responses of the linearized equations to all eigenmodes.

In the following part a method is presented, which filters an initial source vector of the linearized Euler equations such that the remaining source excites solely acoustic modes in the linearized Euler equations. We start with the two-dimensional linearized Euler equations for a uniform mean flow with an additional source term. The extension to non-uniform flows based on the findings in this section will be presented in Section 3.1. In Section 3.4 it will be shown that source filtering is an appropriate method to derive equations, which are stable for arbitrary mean flows and density gradients.

For a uniform mean flow in the x-direction the linearized Euler equations can be written as

$$\frac{\partial \boldsymbol{U}}{\partial t}+\frac{\partial \boldsymbol{E}}{\partial x}+\frac{\partial \boldsymbol{F}}{\partial y}=\boldsymbol{S}, \tag{1}$$

where $\boldsymbol{U}=(\rho,u,v,p)^{\mathrm{T}}$ is the vector of the primitive perturbation variables, i.e., the density ρ, the Cartesian velocity components u,v and the pressure p. $\boldsymbol{E}$ and $\boldsymbol{F}$ are the flux vectors,

$$\boldsymbol{U}=\begin{pmatrix}\rho\\ u\\ v\\ p\end{pmatrix},\quad \boldsymbol{E}=\begin{pmatrix}\rho_\infty u+\rho u_\infty\\ u_\infty u+p/\rho_\infty\\ u_\infty v\\ u_\infty p+\gamma p_\infty u\end{pmatrix},\quad \boldsymbol{F}=\begin{pmatrix}\rho_\infty v\\ 0\\ p/\rho_\infty\\ \gamma p_\infty v\end{pmatrix}, \tag{2}$$

and $\boldsymbol{S}$ can be any arbitrary source. Constant mean flow quantities are denoted by the subscript ∞ and γ represents the ratio of specific heats. As shown in Appendix A, Eq. (1) can be rewritten by combined Fourier and Laplace transformation in the following form:

$$\boldsymbol{A}\widetilde{\boldsymbol{U}}=\widetilde{\boldsymbol{G}}. \tag{3}$$

The transformation changes the time and space dependence into a frequency and wave number dependence, i.e., $f(t,x,y)$ is transferred into $\widetilde{f}(\omega,\alpha,\beta)$, where the quantities α and β denote the wave numbers in the x- and y-direction, respectively. The matrix $\boldsymbol{A}$ is given for the two-dimensional case by Eq. (A.8). Due to the

fact that a Laplace transformation is applied to the time coordinate, initial conditions at time level $t = 0$ can be immediately identified. As shown in Appendix A the source of Eq. (3) is

$$\widetilde{\boldsymbol{G}} = \mathrm{i}(\widetilde{\boldsymbol{S}} + \widetilde{\boldsymbol{U}}_{\text{initial}}/2\pi). \tag{4}$$

The eigenvalues λ_j (A.10) and the eigenvectors $\boldsymbol{x}_j$, $j = 1, \ldots, 4$, (A.11) and (A.12) of the matrix $\boldsymbol{A}$ are related to the eigenmodes of the linearized Euler equations (1). According to the enumeration in Appendix A, the first and second eigenvector are related to entropy and vorticity waves, respectively. The third and fourth eigenvector describe acoustic eigenmodes. The transform of the vector of the primitive variables $\widetilde{\boldsymbol{U}}$ can be expressed as a linear combination of all eigenmodes

$$\widetilde{\boldsymbol{U}} = \frac{C_1}{\lambda_1}\boldsymbol{x}_1 + \frac{C_2}{\lambda_2}\boldsymbol{x}_2 + \frac{C_3}{\lambda_3}\boldsymbol{x}_3 + \frac{C_4}{\lambda_4}\boldsymbol{x}_4 = \boldsymbol{X}\boldsymbol{\Lambda}^{-1} \cdot \boldsymbol{C}. \tag{5}$$

The columns of the matrix $\boldsymbol{X}$ are given by the eigenvectors $\boldsymbol{x}_j$. Furthermore, the matrix of the eigenvalues and its inverse are introduced via

$$\boldsymbol{\Lambda} = \mathrm{diag}(\lambda_1, \ldots, \lambda_4), \quad \boldsymbol{\Lambda}^{-1} = \mathrm{diag}(\lambda_1^{-1}, \ldots, \lambda_4^{-1}).$$

The vector $\boldsymbol{C}$ has the components C_j. By substituting Eq. (5) for $\widetilde{\boldsymbol{U}}$ in Eq. (3) and by applying the similarity transformation $\boldsymbol{A} = \boldsymbol{X}\boldsymbol{\Lambda}\boldsymbol{X}^{-1}$ Eq. (3) can be rewritten

$$\boldsymbol{X}\boldsymbol{C} = \widetilde{\boldsymbol{G}} \tag{6}$$

to yield after multiplying with the inverse of the matrix of the eigenvectors $\boldsymbol{X}^{-1}$ (A.15)

$$\boldsymbol{C} = \boldsymbol{X}^{-1}\widetilde{\boldsymbol{G}}. \tag{7}$$

The components of the vector $\boldsymbol{C}$ describe the response of the various eigenmodes due to the source term $\widetilde{\boldsymbol{G}}$. From Eq. (7) a modified vector can be derived by dropping all but one component of $\boldsymbol{C}$, say, component i of eigenmode i. Introducing this modified vector into Eq. (6) yields a condition for a modified source term, which excites only the ith eigenmode of the governing equations. The computation yields for the source vector of mode i

$$\widetilde{\boldsymbol{G}}_i = \boldsymbol{x}_i\left(\boldsymbol{x}_i^{-1}\right)^{\mathrm{T}}\widetilde{\boldsymbol{G}}, \tag{8}$$

where $(\boldsymbol{x}_i^{-1})^{\mathrm{T}}$ denotes the ith row of the inverse matrix $\boldsymbol{X}^{-1}$. The dyadic product of the $\boldsymbol{x}_i$ vectors in (8) yields a filtering matrix. To be more precise, from the two acoustic eigenmodes $\boldsymbol{x}_3$ and $\boldsymbol{x}_4$ a combined acoustic filtering matrix follows:

$$\boldsymbol{T}^{\mathrm{a}} = \boldsymbol{x}_3\left(\boldsymbol{x}_3^{-1}\right)^{\mathrm{T}} + \boldsymbol{x}_4\left(\boldsymbol{x}_4^{-1}\right)^{\mathrm{T}}, \tag{9}$$

$$\boldsymbol{T}^{\mathrm{a}} = \begin{pmatrix} 0 & 0 & 0 & c_\infty^{-2} \\ 0 & \alpha^2\left(\alpha^2+\beta^2\right)^{-1} & \alpha\beta\left(\alpha^2+\beta^2\right)^{-1} & 0 \\ 0 & \alpha\beta\left(\alpha^2+\beta^2\right)^{-1} & \beta^2\left(\alpha^2+\beta^2\right)^{-1} & 0 \\ 0 & 0 & 0 & 1 \end{pmatrix} \tag{10}$$

that determines an acoustic source vector

$$\widetilde{\boldsymbol{G}}^{\mathrm{a}} = \boldsymbol{T}^{\mathrm{a}} \cdot \widetilde{\boldsymbol{G}}. \tag{11}$$

The inverse transformation of the acoustic source vector into space and time follows by using the formalism given in (A.3). For example, neglecting the initial quantities in Eq. (4), i.e., the full source vector reads

$\widetilde{\boldsymbol{G}} = \mathrm{i}\widetilde{\boldsymbol{S}}$, and using the matrix $\boldsymbol{T}^{\mathrm{a}}$ (10) for the second row of Eq. (11) the following equation in wave number/frequency space is obtained

$$-(\alpha^2+\beta^2)\widetilde{S}_2^{\mathrm{a}} = -\alpha^2\widetilde{S}_2 - \alpha\beta\widetilde{S}_3.$$

Applying (A.3) the solution in time and space reads

$$\left(\frac{\partial^2}{\partial x^2}+\frac{\partial^2}{\partial y^2}\right)S_2^{\mathrm{a}} = \frac{\partial^2}{\partial x^2}S_2 + \frac{\partial^2}{\partial x\partial y}S_3.$$

After the analysis for all components of Eq. (11) a system of differential equations is obtained, which relates the components of the filtered source vector $\boldsymbol{S}^{\mathrm{a}}$ to those of the full source vector $\boldsymbol{S}$

$$S_1^{\mathrm{a}} = c_\infty^{-2}S_4, \tag{12}$$

$$\nabla^2 S_2^{\mathrm{a}} = \frac{\partial^2}{\partial x^2}S_2 + \frac{\partial^2}{\partial x\partial y}S_3, \tag{13}$$

$$\nabla^2 S_3^{\mathrm{a}} = \frac{\partial^2}{\partial x\partial y}S_2 + \frac{\partial^2}{\partial y^2}S_3, \tag{14}$$

$$S_4^{\mathrm{a}} = S_4. \tag{15}$$

The vanishing initial conditions are no severe constraint, since this can be always accomplished by using a source weighting function to initialize the source during a transient process. Except for the factor c_∞^{-2} the first and fourth filtered source component are equal and in conjunction with the linearized Euler equations (1) only isentropic pressure and density fluctuations are excited. The second and third component of the filtered source vector are determined via Poisson equations. The evaluation of these components can be simplified further by defining a source function Φ, which is related to the filtered components via

$$S_2^{\mathrm{a}} = \frac{\partial\Phi}{\partial x}, \quad S_3^{\mathrm{a}} = \frac{\partial\Phi}{\partial y}, \tag{16}$$

such that only one Poisson equation has to be solved using the condition

$$\nabla^2\Phi = \frac{\partial S_2}{\partial x} + \frac{\partial S_3}{\partial y}. \tag{17}$$

Let us summarize the result of this section. An acoustic source vector is determined for the two-dimensional problem with uniform mean flow in the x-direction. This acoustic source follows from a full source vector $\boldsymbol{S} = (S_1, S_2, S_3, S_4)^{\mathrm{T}}$ via

$$\boldsymbol{S}^{\mathrm{a}} = \begin{pmatrix} c_\infty^{-2}S_4 \\ \partial\Phi/\partial x \\ \partial\Phi/\partial y \\ S_4 \end{pmatrix} = \begin{pmatrix} c_\infty^{-2}S_4 \\ \nabla\Phi \\ S_4 \end{pmatrix}, \tag{18}$$

where $\Phi(x,y,t)$ is the solution of Eq. (17). Note that similar to the acoustic filtering matrix (9) additional filtering matrices for the entropy and vorticity modes can be derived. The sum of all matrices yields the unity matrix.

In the three-dimensional problems the acoustic source vector components of the full source vector $\boldsymbol{S} = (S_1, \ldots, S_5)^{\mathrm{T}}$ can also be determined from the gradient of a source function $\Phi(x, y, z, t)$ and a source function of the energy equation S_5, i.e.,

$$\boldsymbol{S}^{\mathrm{a}} = \begin{pmatrix} c_\infty^{-2} S_5 \\ \nabla \Phi \\ S_5 \end{pmatrix}, \tag{19}$$

where the condition for Φ reads $\nabla^2 \Phi = \partial S_2/\partial x + \partial S_3/\partial y + \partial S_4/\partial z$.

3. Acoustic perturbation equations

Various forms of acoustic perturbation equations (APEs) are introduced. First the basic system is derived, which does not contain any vortical modes. Then, the basic system is slightly modified to gain a convenient structure for an incompressible initial flow simulation. Following a stability analysis of the acoustic system the form of the wave operator of the acoustic perturbation equations is used to rewrite the governing equations such that a hydrodynamically stable system with a simple source term for a compressible flow simulation results that is based on the Lamb vector $\boldsymbol{\omega} \times \boldsymbol{u}$.

3.1. Derivation of the fundamental system

The source-term filtering is derived for uniform mean flows. A simple extension to non-uniform mean flows is difficult to achieve since in this case products of mean flow and perturbation quantities in Fourier/Laplace space cannot be separated. Acoustic perturbation equations, however, which also take into account the convection and refraction effects of a non-uniform flow field, can be derived similar to the extension of Lighthill's equation to higher acoustic analogies. Considering exterior flow problems in the inhomogeneous acoustic domain the Lighthill source on the right-hand side describes besides acoustic sources also refraction and convection effects. Convection effects are encoded in the products of mean flow and acoustic perturbation velocities. By shifting those terms to the left-hand wave operator side higher acoustic analogies can be derived. As discussed by Ribner [34] using this procedure an extension of Lighthill's equation in terms of pressure p' can be formulated as a precursor of Lilley's acoustic analogy [25]. To obtain a scalar wave equation for the acoustic variable p' in an additional step the perturbation velocities have to be substituted using the momentum equation.

This concept can also be pursued in the case of the linearized Euler equations for a vanishing mean flow $\boldsymbol{u}_\infty = 0$ with filtered acoustic source vector to achieve a formulation for the non-uniform flow problem. To make convection and refraction effects part of the acoustic field solution the related source terms have to be shifted to the left-hand side. Since in this case no scalar wave equation is solved for one single acoustic variable but rather a system of equations for a complete set of acoustic variables, the second step of substituting the acoustic variable is unnecessary. As shown in Section 2, the acoustic source of the momentum equation is given by the gradient of the source function Φ, which is found by solving the Poisson equation (17). Due to the linearity of the Poisson equation, it can be split into several contributions. To be more precise, a splitting can be introduced such that one part is related to the convection effects. It will be shown below that it is possible to evaluate the convection terms explicitly, if the momentum equation is written in primitive variables. Furthermore, to be able to apply the source-term filtering, the governing equations in primitive variables have to be transformed initially into a system of linear differential equations on the left-hand side with constant coefficients that describe wave propagation in a quiescent or uniformly moving medium. The remaining terms are lumped together as sources on the right-hand side.

A system of differential equations satisfying the previously prescribed constraints can be formulated by using the enthalpy h as variable in the governing equations from which the pressure can be deduced. Then, the continuity and Navier–Stokes equations can be written for a two- or three-dimensional problem with the enthalpy h and the velocities $\boldsymbol{u}$ as variables

$$\frac{\partial h}{\partial t} + c_\infty^2(\nabla \cdot \boldsymbol{u}) = q, \tag{20}$$

$$\frac{\partial \boldsymbol{u}}{\partial t} + \nabla h = \boldsymbol{f}, \tag{21}$$

with

$$q = -\boldsymbol{u} \cdot \nabla h - \left(c^2 - c_\infty^2\right)(\nabla \cdot \boldsymbol{u}) + \frac{c^2}{R}\frac{Ds}{Dt}, \tag{22}$$

$$\boldsymbol{f} = -(\boldsymbol{u} \cdot \nabla)\boldsymbol{u} + \frac{\nabla \cdot \underline{\tau}}{\rho} + T\nabla s. \tag{23}$$

Here, s and $c = \sqrt{\gamma p/\rho}$ represent the entropy and speed of sound, respectively. The stress tensor is denoted by $\underline{\tau}$. The density ρ is substituted using the second law of thermodynamics

$$\frac{\mathrm{d}\rho}{\rho} = \frac{1}{\gamma}\frac{\mathrm{d}p}{p} - \frac{\mathrm{d}s}{c_\mathrm{p}}, \tag{24}$$

which is rewritten for thermally and calorically ideal gas that obeys

$$p = \frac{\gamma - 1}{\gamma} c_\mathrm{p} \rho T. \tag{25}$$

The pressure in the momentum equation is expressed by the enthalpy using the usual form of the second law

$$\frac{\nabla p}{\rho} = \nabla h - T\nabla s. \tag{26}$$

The continuity equation is extended with the identity $c_\infty^2(\nabla \cdot \boldsymbol{u}) = c_\infty^2(\nabla \cdot \boldsymbol{u})$. The left-hand side of the system (20) and (21) can be transformed into a wave equation for the enthalpy h with propagation speed c_∞

$$\left[\frac{\partial^2}{\partial t^2} - c_\infty^2 \nabla^2\right] h = \frac{\partial q}{\partial t} - c_\infty^2 \nabla \cdot \boldsymbol{f}.$$

The left-hand sides of the equation system (20) and (21) have an acoustic and a vorticity eigenmode such that also vorticity waves are excited by the right-hand side. However, due to the chosen set of variables entropy modes are a priori excluded from the system of differential equations. For n-dimensional problems the left-hand side of (20) and (21) is a system of $n+1$ equations for $n+1$ variables $(h, \boldsymbol{u})^\mathrm{T}$, hence it is complete. The right-hand side source also includes entropy fluctuations. Therefore, the source has to be determined from a CFD solution, which also provides the information on entropy fluctuations.

The vorticity eigenmode of the system (20) and (21) describes vortical disturbances occurring in a quiescent medium. Note that the derivation discussed below could also be carried out for a system of equations containing a constant convection speed on the left-hand side, in other words for a system describing wave propagation in a fluid moving at $\boldsymbol{u}_\infty = \text{const}$. Then, the homogeneous system describes

properly the wave propagation in the homogeneous acoustic domain for exterior problems with that free flow velocity. Since the particular value of $\boldsymbol{u}_\infty = \text{const}$ does not affect the final result, for simplicity, the following derivation is discussed for a medium with $\boldsymbol{u}_\infty = 0$.

The constant coefficient c_∞ in Eqs. (20) and (21) allows to apply the source-term filtering to obtain an acoustic source from the combined acoustic and vorticity source $\boldsymbol{S} = (q, \boldsymbol{f})$ on the right-hand side. A filtered source vector, which will excite either acoustical (superscript a) or vortical (superscript v) modes, follows in the wave number/frequency space from the matrix operation

$$\widetilde{\boldsymbol{G}}^{\mathrm{a,v}} = \boldsymbol{T}^{\mathrm{a,v}} \cdot \widetilde{\boldsymbol{G}}, \tag{27}$$

where the tilde denotes transformed quantities. The filtering matrices for the acoustic and the non-acoustic modes in wave number and frequency space is computed according to the procedure described in Section 2. Fourier/Laplace transformation according to Appendix A yields the governing equation system in the form of Eq. (3) with the transformed source vector equation (4). When only two-dimensional problems are considered the matrix $\boldsymbol{A}$ and the vector of the transformed variables $\widetilde{\boldsymbol{U}}$ read for the particular Eqs. (20) and (21)

$$\boldsymbol{A} = \begin{pmatrix} \bar{\omega} & -c_\infty^2\alpha & -c_\infty^2\beta \\ -\alpha & \bar{\omega} & 0 \\ -\beta & 0 & \bar{\omega} \end{pmatrix}, \quad \widetilde{\boldsymbol{U}} = \begin{pmatrix} \widetilde{h} \\ \widetilde{u} \\ \widetilde{v} \end{pmatrix}. \tag{28}$$

The eigenvalues are $\lambda_1 = \bar{\omega}$, $\lambda_{2,3} = \bar{\omega} \mp \sqrt{\alpha^2 + \beta^2}$, and the related eigenvectors $\boldsymbol{x}_i$ determine the columns of the matrix $\boldsymbol{X}$

$$\boldsymbol{X} = (\boldsymbol{x}_1, \boldsymbol{x}_2, \boldsymbol{x}_3) = \begin{pmatrix} 0 & 1 & 1 \\ \beta & \alpha/(c_\infty\sqrt{\alpha^2+\beta^2}) & -\alpha/(c_\infty\sqrt{\alpha^2+\beta^2}) \\ -\alpha & \beta/(c_\infty\sqrt{\alpha^2+\beta^2}) & -\beta/(c_\infty\sqrt{\alpha^2+\beta^2}) \end{pmatrix}.$$

The first eigenvector $\boldsymbol{x}_1$ defines the vorticity mode, while the other eigenvectors $\boldsymbol{x}_2$, $\boldsymbol{x}_3$ describe acoustic modes. The inverse of $\boldsymbol{X}$, i.e., $\boldsymbol{X}^{-1}$, whose rows are denoted by $(\boldsymbol{x}_i^{-1})^{\mathrm{T}}$ reads

$$\boldsymbol{X}^{-1} = \begin{pmatrix} (\boldsymbol{x}_1^{-1})^{\mathrm{T}} \\ (\boldsymbol{x}_2^{-1})^{\mathrm{T}} \\ (\boldsymbol{x}_3^{-1})^{\mathrm{T}} \end{pmatrix} = \begin{pmatrix} 0 & \beta/(\alpha^2+\beta^2) & -\alpha/(\alpha^2+\beta^2 \\ 1/2 & \alpha c_\infty/\left(2\sqrt{\alpha^2+\beta^2}\right) & \beta c_\infty/\left(2\sqrt{\alpha^2+\beta^2}\right) \\ 1/2 & -\alpha c_\infty/\left(2\sqrt{\alpha^2+\beta^2}\right) & -\beta c_\infty/\left(2\sqrt{\alpha^2+\beta^2}\right) \end{pmatrix}.$$

The filtering matrices for pure acoustic and vorticity excitation are determined by evaluating $\boldsymbol{T}^{\mathrm{a}} = \boldsymbol{x}_2(\boldsymbol{x}_2^{-1})^{\mathrm{T}} + \boldsymbol{x}_3(\boldsymbol{x}_3^{-1})^{\mathrm{T}}$ and $\boldsymbol{T}^{\mathrm{v}} = \boldsymbol{x}_1(\boldsymbol{x}_1^{-1})^{\mathrm{T}}$, respectively

$$\boldsymbol{T}^{\mathrm{a}} = \begin{pmatrix} 1 & 0 & 0 \\ 0 & \frac{\alpha^2}{\alpha^2+\beta^2} & \frac{\alpha\beta}{\alpha^2+\beta^2} \\ 0 & \frac{\alpha\beta}{\alpha^2+\beta^2} & \frac{\beta^2}{\alpha^2+\beta^2} \end{pmatrix}, \quad \boldsymbol{T}^{\mathrm{v}} = \begin{pmatrix} 0 & 0 & 0 \\ 0 & \frac{\beta^2}{\alpha^2+\beta^2} & -\frac{\alpha\beta}{\alpha^2+\beta^2} \\ 0 & -\frac{\alpha\beta}{\alpha^2+\beta^2} & \frac{\alpha^2}{\alpha^2+\beta^2} \end{pmatrix}. \tag{29}$$

The acoustic source vector in time and space follows from the inverse transformation of Eq. (27) using the acoustic filtering matrix $\boldsymbol{T}^{\mathrm{a}}$ of (29). This procedure agrees with that in Section 2 where Eq. (11) was the starting point of the derivation of the acoustic source equation (18). The components of the filtered acoustic source term in time and space $\boldsymbol{S}^{\mathrm{a}} = (q^{\mathrm{a}}, \boldsymbol{f}^{\mathrm{a}})^{\mathrm{T}}$ follows to be related to the initial source vector $\boldsymbol{S} = (q, \boldsymbol{f})^{\mathrm{T}}$ with the components given in Eqs. (22) and (23) via

$$\boldsymbol{S}^{\mathrm{a}} = \begin{pmatrix} q^{\mathrm{a}} \\ \boldsymbol{f}^{\mathrm{a}} \end{pmatrix} = \begin{pmatrix} q \\ \nabla \Phi \end{pmatrix} \quad \text{with } \nabla^2 \Phi = \nabla \cdot \boldsymbol{f}. \tag{30}$$

The vector $\boldsymbol{S}^{\mathrm{a}}$ excites Eqs. (20) and (21) and generates only responses of the acoustic eigenmodes. That is, on the left-hand side the enthalpy h and the unsteady acoustic velocities $\boldsymbol{u}_i$ are excited

$$\frac{\partial h}{\partial t} + c_\infty^2 (\nabla \cdot \boldsymbol{u}_i) = q^{\mathrm{a}}, \tag{31}$$

$$\frac{\partial \boldsymbol{u}_i}{\partial t} + \nabla h = \boldsymbol{f}^{\mathrm{a}}. \tag{32}$$

Note that the discussion below will show the enthalpy h not to be split by the source filtering. Taking the curl of Eq. (32) with $\boldsymbol{f}^{\mathrm{a}} = \nabla \Phi$ yields

$$\frac{\partial}{\partial t} (\nabla \times \boldsymbol{u}_i) = 0 \tag{33}$$

such that the decomposed velocity $\boldsymbol{u}_i$ remains irrotational if it is initially irrotational. Since the derivation of the source filtering assumes vanishing initial conditions, see Section 2, this constraint is satisfied. Furthermore, it follows from the filtered vorticity source $\boldsymbol{S}^{\mathrm{v}}$, that it induces on the left-hand side of Eq. (21) a solenoidal velocity field $\boldsymbol{u}_{\mathrm{s}}$. Since the sum of the filtering matrices (29) yields the unity matrix, the sum of Eq. (32) with acoustic source plus the related equation for the vortical mode must yield Eq. (21) with source equation (23). That is, in restating the Helmholtz decomposition theorem using the source filtering the velocity is split uniquely into an irrotational and a solenoidal part, i.e.,

$$\boldsymbol{u} = \boldsymbol{u}_{\mathrm{i}} + \boldsymbol{u}_{\mathrm{s}}. \tag{34}$$

Due to the source filtering, the irrotational velocity $\boldsymbol{u}_{\mathrm{i}}$, which could also contain non-zero time averaged velocity components, is completely related to the acoustic mode.

In the following a system of acoustic equations for perturbation quantities for a non-vanishing mean flow is derived. The perturbations are defined to be deviations from time-averaged mean quantities

$$\boldsymbol{u} = \bar{\boldsymbol{u}} + \boldsymbol{u}' = \bar{\boldsymbol{u}} + \boldsymbol{u}^{\mathrm{v}} + \boldsymbol{u}^{\mathrm{a}}. \tag{35}$$

Here $\bar{\boldsymbol{u}}$ denotes the time-averaged mean flow, $\boldsymbol{u}^{\mathrm{v}}$ is a solenoidal vortical perturbation, and $\boldsymbol{u}^{\mathrm{a}}$ is an irrotational acoustic perturbation. First, Eq. (32) is considered. The irrotational velocity $\boldsymbol{u}_{\mathrm{i}}$ occurs only as a time derivative on the left-hand side, thus the irrotational perturbation velocity $\boldsymbol{u}^{\mathrm{a}}$ can be substituted for $\boldsymbol{u}_{\mathrm{i}}$. To transfer terms, which describe convection effects, to the left-hand side of Eq. (32) the decomposition of Eq. (35) $\bar{\boldsymbol{u}} + \boldsymbol{u}^{\mathrm{v}} + \boldsymbol{u}^{\mathrm{a}}$ is substituted for the velocity $\boldsymbol{u}$ in the source term. Convection of the acoustic disturbances by the mean flow is described by the terms containing mean and acoustic perturbation velocities. Due to the linearity of the Poisson in Eq. (30) Φ can be split into three parts $\Phi_1 + \Phi_2 + \Phi_{\mathrm{P}}$, where the first part is determined by the acoustic/mean velocity terms, the second is determined by the terms containing the enthalpy and the entropy, and the third part is described by the remaining terms. The analysis leads to

$$\nabla^2 \Phi_1 = -\nabla \cdot \left[(\bar{\boldsymbol{u}} \cdot \nabla) \boldsymbol{u}^{\mathrm{a}} + (\boldsymbol{u}^{\mathrm{a}} \cdot \nabla) \bar{\boldsymbol{u}} \right], \tag{36}$$

$$\nabla^2 \Phi_2 = -\nabla \cdot \left[-\nabla \bar{h} - (T \nabla s)' \right], \tag{37}$$

$$\nabla^2 \Phi_{\mathrm{P}} = -\nabla \cdot \left[(\bar{\boldsymbol{u}} \cdot \nabla)\boldsymbol{u}^{\mathrm{v}} + (\boldsymbol{u}^{\mathrm{v}} \cdot \nabla)\bar{\boldsymbol{u}} + ((\boldsymbol{u}^{\mathrm{v}} \cdot \nabla)\boldsymbol{u}^{\mathrm{v}})' - \left(\frac{\nabla \cdot \underline{\tau}}{\rho} \right)' \right]. \tag{38}$$

To obtain Eqs. (36)–(38) all non-linear terms containing the acoustic velocity $\boldsymbol{u}^{\mathrm{a}}$ are dropped. Furthermore, the time-averaged version of Eq. (21) and (23) has been used, i.e.,

$$\left(\bar{\boldsymbol{u}} \cdot \nabla\right)\bar{\boldsymbol{u}} = -\nabla \bar{h} + \overline{T \nabla s} - \overline{(\boldsymbol{u}' \cdot \nabla)\boldsymbol{u}'} + \overline{\left(\frac{\nabla \cdot \underline{\tau}}{\rho} \right)} \tag{39}$$

to eliminate the term $(\bar{\boldsymbol{u}} \cdot \nabla)\bar{\boldsymbol{u}}$ in the source. Throughout the remaining part of this work primed terms in parentheses denote $(\cdots)' = (\cdots) - \overline{(\cdots)}$. Using the relation

$$(\bar{\boldsymbol{u}} \cdot \nabla)\boldsymbol{u}^{\mathrm{a}} + (\boldsymbol{u}^{\mathrm{a}} \cdot \nabla)\bar{\boldsymbol{u}} = \nabla\left(\bar{\boldsymbol{u}} \cdot \boldsymbol{u}^{\mathrm{a}}\right) + \bar{\boldsymbol{\omega}} \times \boldsymbol{u}^{\mathrm{a}}, \tag{40}$$

which follows from an identity plus exploiting the irrotationality of the acoustic perturbation velocity, i.e., $\boldsymbol{\omega}^{\mathrm{a}} = \nabla \times \boldsymbol{u}^{\mathrm{a}} = 0$, the Poisson equation (36) can be explicitly evaluated

$$\nabla \Phi_1 = -\nabla\left(\bar{\boldsymbol{u}} \cdot \boldsymbol{u}^{\mathrm{a}}\right) + \nabla q_{\bar{\omega}}, \tag{41}$$

where $\nabla q_{\bar{\omega}}$ contains all remaining terms and follows from

$$\nabla^2 q_{\bar{\omega}} = -\nabla \cdot \left(\bar{\boldsymbol{\omega}} \times \boldsymbol{u}^{\mathrm{a}}\right). \tag{42}$$

Since $T \nabla s = \nabla Q$, where Q represents the specific heat, this term and its time average is irrotational such that the complete Poisson equation (37) can be explicitly solved

$$\nabla \Phi_2 = \nabla \bar{h} + \bar{T} \nabla s' + T' \nabla \bar{s}. \tag{43}$$

The entropy fluctuations are considered in the source only to first-order, hence, the entropy terms of Eq. (37) appear as $(T \nabla s)' \approx \bar{T} \nabla s' + T' \nabla \bar{s}$. Next, the explicitly given terms of Eq. (41) and the mean enthalpy of Eq. (43) are shifted to the left-hand side of Eq. (32) and the perturbation pressure $p' = p - \bar{p}$ is substituted for the perturbation enthalpy $h' = h - \bar{h}$ using the first-order formulation of the second law of thermodynamics, i.e.,

$$h' = \frac{p'}{\bar{\rho}} + \bar{T} s', \tag{44}$$

to obtain a governing equation for the acoustic perturbation velocity

$$\frac{\partial \boldsymbol{u}^{\mathrm{a}}}{\partial t} + \nabla\left(\bar{\boldsymbol{u}} \cdot \boldsymbol{u}^{\mathrm{a}}\right) + \nabla\left(\frac{p'}{\bar{\rho}}\right) = \nabla \Phi_{\mathrm{P}} + \nabla q_{\bar{\omega}} + T' \nabla \bar{s} - s' \nabla \bar{T}.$$

Let us turn now to Eq. (31) with the acoustic source equation (30). The source-term filtering leaves the source unchanged, i.e., $q^{\mathrm{a}} = q$. Using the decomposition given in Eq. (34), where $\boldsymbol{u}_{\mathrm{s}}$ is solenoidal, it can be evidenced that $\nabla \cdot \boldsymbol{u}$ can be substituted for $\nabla \cdot \boldsymbol{u}_i$ on the left-hand side of Eq. (31). Hence, the source-filtered equation (31) remains unchanged compared with the original Eq. (20) with source equation (22). Since this equation is a governing equation for the enthalpy h, this result means that the acoustic source filtering does not yield a splitting of the enthalpy and as such the enthalpy is completely related to the acoustic eigenmode.

The governing equation for the acoustic velocity perturbations was rewritten using the perturbation pressure p' as variable. Accordingly, Eq. (20) with source equation (22) is rewritten as governing equation

for p'. Since the entropy was assumed to be a known quantity, it is valid to use the continuity equation with the density ρ as variable instead of Eqs. (20) and (22). Neglecting the non-linear acoustic terms the continuity equation can be rewritten in terms of the perturbation density $\rho' = \rho - \bar{\rho}$ using the decomposition (35)

$$\frac{\partial \rho'}{\partial t} + \nabla \cdot \left(\bar{\rho} \boldsymbol{u}^{\mathrm{a}} + \rho' \bar{\boldsymbol{u}} \right) = -\nabla \cdot (\rho \boldsymbol{u}^{\mathrm{v}}). \tag{45}$$

The perturbation density in Eq. (45) is replaced by the perturbation pressure via the fist-order form of Eq. (24)

$$p' - \bar{c}^2 \rho' = \frac{\gamma \bar{p}}{c_{\mathrm{p}}} s'. \tag{46}$$

Then, the complete system of acoustic perturbation equations (APEs) for the perturbation variables $(p', \boldsymbol{u}^{\mathrm{a}})^{\mathrm{T}}$ reads

$$\frac{\partial p'}{\partial t} + \bar{c}^2 \nabla \cdot \left(\bar{\rho} \boldsymbol{u}^{\mathrm{a}} + \bar{\boldsymbol{u}} \frac{p'}{\bar{c}^2} \right) = \bar{c}^2 q_c, \tag{47}$$

$$\frac{\partial \boldsymbol{u}^{\mathrm{a}}}{\partial t} + \nabla \left(\bar{\boldsymbol{u}} \cdot \boldsymbol{u}^{\mathrm{a}} \right) + \nabla \left(\frac{p'}{\bar{\rho}} \right) = \boldsymbol{q}_m \tag{48}$$

with sources

$$q_c = \underbrace{-\nabla \rho \cdot \boldsymbol{u}^{\mathrm{v}}}_{\mathrm{I}} + \underbrace{\frac{\bar{\rho}}{c_{\mathrm{p}}} \frac{\bar{D} s'}{Dt}}_{\mathrm{II}}, \tag{49}$$

$$\boldsymbol{q}_m = \underbrace{\nabla \Phi_{\mathrm{P}}}_{\mathrm{III}} + \underbrace{\nabla q_{\bar{\omega}}}_{\mathrm{IV}} + \underbrace{T' \nabla \bar{s} - s' \nabla \bar{T}}_{\mathrm{V}}, \tag{50}$$

where $\bar{D}/Dt = \partial/\partial t + \bar{\boldsymbol{u}} \cdot \nabla$ denotes the substantial time derivative. The system (47) and (48) plus sources (49) and (50) is the basic result of this section and forms the basis for noise prediction.

The system describes wave propagation in a non-uniform mean flow field $\bar{\boldsymbol{u}}$. In the derivation the non-linear terms containing acoustic perturbations have been dropped, hence non-linear acoustic propagation and sound generation effects due to non-linear mode interaction are not considered by the system. The right-hand side terms q_c and $\boldsymbol{q}_m$ are to be understood as the acoustic sources. Computing the propagation of acoustic waves including convection effects in a time-averaged steady flow field allows to restrict the expensive unsteady flow simulation just to the immediate vicinity of the acoustic source region under consideration, while the mean flow field can be computed using efficient RANS or Euler methods.

Since some variants of the acoustic perturbation equations will be derived in Sections 3.3 and 3.5, this fundamental set of Eqs. (47) and (48) is termed APE-1.

3.2. Discussion of the APE-1 system

The sources of the APE system (49) and (50) labeled with Roman numbers have to be determined from an initial unsteady flow simulation, e.g., based on a large eddy simulation. The source terms I and III are a function of the solenoidal perturbation velocity $\boldsymbol{u}^{\mathrm{v}}$, while the terms II and V involve entropy fluctuations. Since the solenoidal velocity perturbations can be related to turbulent fluctuations, the terms I, II, III, and

V can be deemed sound sources being generated from turbulent fluctuations and entropy inhomogeneities. The remaining source term IV is a function of the mean flow vorticity $\bar{\boldsymbol{\omega}}$ and the acoustic perturbation velocity $\boldsymbol{u}^{\mathrm{a}}$, which follows from the solution of the Poisson problem (42). This term describes sound generation due to acoustic/mean–vorticity interaction. Since for external flow problems the wave propagation occurs mainly in areas with small mean flow vorticity, i.e., outside boundary layers where the flow field is sufficiently accurately described by a velocity potential, this term might be negligible. The importance of this term when wave propagation in a mean flow with evident vorticity is computed will be addressed in Section 4.2.

The source term II of the continuity equation (47) describes a monopolar heat source. Since it involves the substantial time derivative, entropy disturbances convecting with the mean flow do not generate sound. If combustion noise is considered this term as well as term V that also involves entropy and temperature fluctuations are important, however, they are assumed to be negligible for vortex sound.

The terms I and III are the major source terms for turbulent induced or vortex sound. Term III is determined by the solution of the Poisson problem (38). For small Mach numbers, i.e., in the limit $M \to 0$, the unsteady flow field is completely defined by the solenoidal perturbation velocity $\boldsymbol{u}^{\mathrm{v}}$, if only non-porous wall boundaries are considered. This property is used, e.g., in the vorticity-streamfunction approach for the simulation of incompressible flows, where the velocity field is described by a streamfunction. The right-hand side of Eq. (38) can be expanded by the time derivative of the solenoidal perturbation velocity since $\nabla \cdot \partial \boldsymbol{u}^{\mathrm{v}}/\partial t$ vanishes. Thus, the Poisson equation can be rewritten as

$$\nabla^2 \Phi_{\mathrm{P}} = -\nabla \cdot \left[\frac{\partial \boldsymbol{u}^{\mathrm{v}}}{\partial t} + (\overline{\boldsymbol{u}} \cdot \nabla)\boldsymbol{u}^{\mathrm{v}} + (\boldsymbol{u}^{\mathrm{v}} \cdot \nabla)\overline{\boldsymbol{u}} + ((\boldsymbol{u}^{\mathrm{v}} \cdot \nabla)\boldsymbol{u}^{\mathrm{v}})' - \left(\frac{\nabla \cdot \underline{\tau}}{\rho} \right)' \right].$$

As can be seen from the terms in brackets on the right-hand side for small Mach numbers, i.e., $M \ll 1$, the quantity Φ_{P} is equal to P'/ρ_∞, where $P' = P - \overline{P}$ is the incompressible perturbation pressure. Furthermore, $\rho \to \rho_\infty$ and $\nabla\rho \to 0$ holds such that the source term I drops in this limit. That is, in the low Mach number limit and when entropy effects are discarded and only vortex sound is considered the major source term is III. If an incompressible large eddy simulation has been carried out this term can be immediately evaluated using the incompressible perturbation pressure P', i.e.,

$$\nabla \Phi_{\mathrm{P}} \simeq \frac{\nabla P'}{\rho_\infty}. \tag{51}$$

3.3. APE variant 2

In this section the application of the acoustic perturbation equations (APEs) in conjunction with acoustic sources from an incompressible unsteady flow simulation is discussed. The system (47) and (48) with sources (49) and (50) is reformulated such that the time derivative of Φ_{P} from term III appears as a source term. In order to achieve this, the perturbation pressure must be decomposed according to

$$p' = \bar{\rho}\Phi_{\mathrm{P}} + p^{\mathrm{a}}. \tag{52}$$

This decomposition means that the hydrodynamic perturbation pressure $P' \approx \bar{\rho}\Phi_{\mathrm{P}}$ is excluded from the pressure fluctuations p'. Hence, the remaining perturbation pressure p^{a} can be understood as an acoustic perturbation pressure with pseudosound excluded. Note that the decomposition, which formally follows from the source-term filtering, relates the complete perturbation pressure to the acoustic mode. Using this decomposition (52) and Eqs. (45) and (46) instead of Eq. (47) a modified acoustic perturbation system follows:

$$\frac{\partial \rho'}{\partial t} + \nabla \cdot \left(\rho' \bar{\boldsymbol{u}} + \bar{\rho} \boldsymbol{u}^{\mathrm{a}} \right) = -\nabla \bar{\rho} \cdot \boldsymbol{u}^{\mathrm{v}}, \tag{53}$$

$$\frac{\partial \boldsymbol{u}^{\mathrm{a}}}{\partial t} + \nabla \left(\bar{\boldsymbol{u}} \cdot \boldsymbol{u}^{\mathrm{a}} \right) + \nabla \left(\frac{p^{\mathrm{a}}}{\bar{\rho}} \right) = \nabla q_{\bar{\omega}} + T' \nabla \bar{s} - \nabla \bar{T} s', \tag{54}$$

$$\frac{\partial p^{\mathrm{a}}}{\partial t} - \bar{c}^2 \frac{\partial \rho'}{\partial t} = \underbrace{-\bar{\rho} \frac{\partial \Phi_{\mathrm{P}}}{\partial t}}_{\mathrm{IIIb}} + \underbrace{\frac{\gamma \bar{p}}{c_{\mathrm{p}}} \frac{\partial s'}{\partial t}}_{\mathrm{IIb}}. \tag{55}$$

This new formulation of the acoustic perturbation equations will be termed APE-2. The heat source IIb in the formulation of the APE-2 system is directly related to the perturbed heat release per unit volume Q' [W/m^3] via

$$\mathrm{IIb} = \frac{\bar{\rho}}{c_{\mathrm{p}}} \frac{\partial s'}{\partial t} = \frac{(\gamma - 1)}{\bar{c}^2} \frac{\partial Q'}{\partial t}.$$

Considering only vortex sound at small Mach numbers and neglecting the linear coupling between the acoustic and vorticity mode, that is described by the source $q_{\bar{\omega}}$, all source terms but IIIb disappear, which in the small Mach number limit can be replaced by the time derivative of the perturbation pressure of an incompressible flow simulation, i.e.,

$$\mathrm{IIIb} = \bar{\rho} \frac{\partial \Phi_{\mathrm{P}}}{\partial t} \simeq \frac{\partial P'}{\partial t}. \tag{56}$$

The perturbation equations (47) and (48) have been derived to prevent the excitation of hydrodynamic instabilities by excluding all vortical modes. The starting point was a system of equations (20) and (21), which excluded entropy modes a priori. By substituting the perturbation density in Eq. (53) for the perturbation pressure in Eq. (47) and by using an additional Eq. (55) to close the system the excluded entropy modes are reintroduced. However, we will evidence in Section 3.4 that the entropy mode does not affect the stability of the system of equations.

In Section 4.4 it will be shown that the source term III or IIIb, respectively, cannot be expressed by the perturbation pressure P' of a compressible flow simulation since the perturbation pressure solution contains acoustic signals that generate additional acoustic responses that are not based on the correct incompressible pressure. These artificial acoustic signals have a large magnitude since the acoustic signals in the source are small but decay only slowly towards the far field. It is shown in Section 4.4 that they cannot be avoided even if a spatial filtering is applied to separate the important hydrodynamic near-field fluctuations from the acoustic far field fluctuations in the source.

However, for the low Mach number flow simulation based on an incompressible approach the APE-2 formulation with the source IIIb is most appropriate, since the vortex sound source based on the time derivative of the incompressible pressure can be determined easily.

To associate the APE system with a compressible flow simulation the unsteady solenoidal perturbation velocity field $\boldsymbol{u}^{\mathrm{v}}$ must be computed via Biot–Savart's law from the unsteady perturbation vorticity field by solving a Poisson problem. The solution of equation (38) yields the source terms III or IIIb. Note that this procedure is not restricted to small Mach number problems.

Although the effort to solve the Poisson problems seems to be comparable to the computational time necessary to advance the APE system, a simpler way to adapt the APE system to a compressible flow simulation would be desirable. One formulation termed APE-3 was introduced in [10] that is based on the perturbed total enthalpy as acoustic variable. Compared with the APE-1 formulation the APE-3 system

possesses the advantage that no Poisson equation has to be solved to determine the source terms. However, an advanced formulation will be given in Section 3.5, termed APE-4, that is based on the usual set of primitive variables, i.e., perturbation pressure and velocities.

3.4. Stability of the acoustic perturbation equations

Although the filtered sources, Eqs. (49) and (50), excite just acoustic modes in the APE-1 system, Eqs. (47) and (48), it is to be noted that the homogeneous APE-1 system has a certain degree of freedom to describe also non-acoustic modes. Instabilities of the homogeneous system could be caused by any eigenmode. However, it will shown in this section that the APE systems are stable for arbitrary mean flows. Note that stability is a property of the acoustic perturbation system that is derived by applying the source filtering procedure and by shifting convection terms to the left-hand side. This essential property is not achieved by suppressing vorticity in the non-homogeneous system through the remaining filtered sources on the right-hand side. In particular, the inverse Laplace transform step of the combined inverse Fourier/Laplace transform equation (A.6), which yields an analytically filtered acoustic source vector in time and space from the transform equation (27), was defined to run above all poles of the integrand. This definition ensures causality of the eigenmodes of the Euler equations in time and space whose combined transform is given by Eq. (A.13). However, the particular choice of the integration path has no influence on the resulting acoustic source vector, hence stability does not depend on it.

Since the acoustic velocity $\boldsymbol{u}^{\mathrm{a}}$, which is generated in response to the filtered source in the APE system, is irrotational, it can be expressed through a potential, i.e.,

$$\boldsymbol{u}^{\mathrm{a}} = \nabla\varphi'. \tag{57}$$

This can be evidenced by taking the curl of Eq. (48), which yields the integrability condition

$$\nabla \times \boldsymbol{u}^{\mathrm{a}} = 0 \tag{58}$$

($\boldsymbol{u}^{\mathrm{a}}(t=0) = 0$, Section 2 [1]). However, to study all eigenmodes of the homogeneous system (47) and (48) it is necessary to perform the analysis for perturbation velocities $\boldsymbol{u}'$, which are allowed to describe irrotational as well as rotational perturbations, i.e.,

$$\frac{\partial p'}{\partial t} + \bar{c}^2\nabla\cdot\left(\bar{\rho}\boldsymbol{u}' + \bar{\boldsymbol{u}}\frac{p'}{\bar{c}^2}\right) = 0, \tag{59}$$

$$\frac{\partial \boldsymbol{u}'}{\partial t} + \nabla\left(\bar{\boldsymbol{u}}\cdot\boldsymbol{u}'\right) + \nabla\left(\frac{p'}{\bar{\rho}}\right) = \boldsymbol{0}. \tag{60}$$

The perturbation velocity $\boldsymbol{u}'$ can be split into an irrotational $\nabla\varphi$ plus a remaining part $\boldsymbol{u}^{\mathrm{r}}$ that contains the complete vorticity

$$\boldsymbol{u}' = \nabla\varphi + \boldsymbol{u}^{\mathrm{r}}. \tag{61}$$

Since $\boldsymbol{u}^{\mathrm{r}}$ is not defined to be solenoidal, the decomposition becomes uniquely defined after imposing the additional condition that the unsteady pressure is expressed only in terms of the unsteady potential φ by

$$p' = -\bar{\rho}\frac{\bar{D}\varphi}{Dt}, \tag{62}$$

[1] Note that the right-hand side of Eq. (48) is irrotational.

with the substantial time derivative $\bar{D}/Dt = \partial/\partial t + \bar{\boldsymbol{u}} \cdot \nabla$. Introducing Eqs. (61) and (62) into Eq. (59) yields a scalar wave equation for φ

$$\mathscr{L}\varphi = \nabla \cdot \left(\bar{\rho} \nabla \varphi - \frac{\bar{\rho}}{\bar{c}^2} \frac{\bar{D}\varphi}{Dt} \bar{\boldsymbol{u}} \right) - \frac{\partial}{\partial t} \left(\frac{\bar{\rho}}{\bar{c}^2} \frac{\bar{D}\varphi}{Dt} \right) = -\nabla \cdot (\bar{\rho} \boldsymbol{u}^{\mathrm{r}}). \tag{63}$$

Using the mean flow relation $\nabla \cdot (\bar{\rho}\bar{\boldsymbol{u}}) = 0$ to simplify the wave (63) and inserting Eqs. (61) and (62) into Eq. (60), the APE-1 system can be rewritten as the equivalent system

$$\mathscr{L}'\varphi = \left[\frac{\bar{D}}{Dt} \left(\frac{1}{\bar{c}^2} \frac{\bar{D}}{Dt} \right) - \frac{1}{\bar{\rho}} \nabla \cdot \left(\bar{\rho} \nabla \right) \right] \varphi = \frac{1}{\bar{\rho}} \nabla \cdot \left(\bar{\rho} \boldsymbol{u}^{\mathrm{r}} \right), \tag{64}$$

$$\frac{\partial \boldsymbol{u}^{\mathrm{r}}}{\partial t} + \nabla \left(\bar{\boldsymbol{u}} \cdot \boldsymbol{u}^{\mathrm{r}} \right) = \boldsymbol{0} \tag{65}$$

for the variables $(\varphi, \boldsymbol{u}^{\mathrm{r}})^{\mathrm{T}}$, where each equation describes the behavior of one eigenmode of the APE-1 system. The convected wave operator $\mathscr{L}'$ for the variable φ of Eq. (64) governs the acoustic mode. Eq. (65) describes the behavior of the vortical perturbations in the APE-1 system. Taking the curl of this equation yields the vorticity equation of the APE-1 system

$$\frac{\partial \boldsymbol{\omega}'}{\partial t} = 0. \tag{66}$$

Since the APE-1 system is derived to be well suited for the simulation of solely acoustic modes it differs from the linearized Euler equations as it does not possess the convection property for the vorticity perturbations. Even for the homogeneous APE-1 system the wave equation of the equivalent system (64) and (65) is coupled with the vorticity equation in a non-uniform mean flow field with density gradients. Nevertheless, it is evident that the vorticity equation (66) is stable. It will be discussed below that the wave operator $\mathscr{L}'$ is stable for arbitrary mean flow fields and thus this result also holds for the equivalent APE-1 system.

Note that the homogeneous linearized Euler equations could also be recast into an equivalent system, where each equation is related to one eigenmode of the system. If the entropy eigenmode is suppressed by demanding the perturbation pressure and density to describe homentropic fields, the coupled acoustic/vortical system of equations corresponds to that proposed by Goldstein [13] and recently used by Golubev and Atassi [14] and by Cooper and Peake [3] to predict the propagation of acoustic disturbances in swirling flows. The inhomogeneous wave operator that governs the acoustic mode agrees with Eq. (64), but the equation for $\boldsymbol{u}^{\mathrm{r}}$

$$\frac{\partial \boldsymbol{u}^{\mathrm{r}}}{\partial t} + \left(\bar{\boldsymbol{u}} \cdot \nabla \right) \boldsymbol{u}^{\mathrm{r}} + (\boldsymbol{u}^{\mathrm{r}} \cdot \nabla) \bar{\boldsymbol{u}} = -\bar{\boldsymbol{\omega}} \times \nabla \varphi \tag{67}$$

also describes growing instability waves, i.e., the equivalent linearized Euler equation are unstable for certain non-uniform mean flows.

The wave operator $\mathscr{L}'$ on the left-hand side of Eq. (64) is that of Pierce's approximate wave equation [31], which was also derived by Goldstein in [13] and recently used in [3,14]. The wave operator is equivalent to the linearized wave operator of Möhring's acoustic analogy [19,27,28], which reads

$$\mathscr{L}'B = \frac{D}{Dt} \left(\frac{1}{c^2} \frac{DB}{Dt} \right) - \frac{1}{\rho} \nabla \cdot (\rho \nabla B) = -\frac{q_{\mathrm{tot}}}{\rho}, \tag{68}$$

where B is the total enthalpy. As discussed by Howe [18] for homentropic high Reynolds number flows his acoustic analogy [20] agrees with Eq. (68).

A great number of various acoustic analogies have been proposed in the past in order to extend Lighthill's acoustic analogy [24] to take into account refraction and convection effects in the wave operator and to identify the real acoustic sources. As discussed by Möhring [27,28] and Bergliaffa et al. [1], the wave operator $\mathscr{L}'$ has some unique features. Bergliaffa et al. [1] derived it from an action principle. As outlined by Möhring [27,28] the wave operator $\mathscr{L}'$ can be shown to be formally self-adjoint. From the self-adjointness a reciprocity relation for the Green's function associated with $\mathscr{L}'$ can be derived. Furthermore, from the self-adjointness one can conclude the existence of a variational principle from which the wave equation (63) can be derived. From the variational principle a conservation law for the acoustic energy can be deduced due to Noether's theorem.

Möhring [27,28] concludes from the energy theorem that for initial value problems with vanishing right-hand side q_{tot} and for a vanishing solution at large distances from the source region the total energy in the sound field remains constant. Since the total energy is a sum of positive contributions, none of these can grow exponentially in time, i.e., instabilities cannot occur.

Since the wave operator $\mathscr{L}'$ can be proven to be stable, it follows that also the APE-1 system is stable. This is a remarkable result since it is neither restricted to a particular class of mean flows, e.g., shear flows, nor limited to constant mean flow densities.

The homogeneous APE-2 system (53) and (55) also allows the occurrence of entropy disturbances. To check whether the system of equations remains stable in this case the governing equations can be split into the equivalent system (64) and (65) plus a governing equation for the entropy mode. To achieve this set of equations the perturbation density ρ' is split into an isentropic ρ^{a} plus a remaining part ρ^{r}, i.e.,

$$\rho' = \rho^{\text{a}} + \rho^{\text{r}}. \tag{69}$$

The isentropic part is related to the perturbation pressure via $p^{\text{a}} - \bar{c}^2\rho^{\text{a}} = 0$. Inserting the decomposition into the homogeneous version of Eqs. (53)–(55), i.e., the right-hand side sources are dropped, yields the equivalent system

$$\left[\frac{\bar{D}}{Dt}\left(\frac{1}{\bar{c}^2}\frac{\bar{D}}{Dt}\right) - \frac{1}{\bar{\rho}}\nabla\cdot\left(\bar{\rho}\nabla\right)\right]\varphi = \frac{1}{\bar{\rho}}\nabla\cdot\left(\bar{\rho}\boldsymbol{u}^{\text{r}} + \rho^{\text{r}}\bar{\boldsymbol{u}}\right), \tag{70}$$

$$\frac{\partial \boldsymbol{u}^{\text{r}}}{\partial t} + \nabla\left(\bar{\boldsymbol{u}}\cdot\boldsymbol{u}^{\text{r}}\right) = \boldsymbol{0}, \tag{71}$$

$$\frac{\partial \rho^{\text{r}}}{\partial t} = 0 \tag{72}$$

for the variables $(\varphi, \boldsymbol{u}^{\text{r}}, \rho^{\text{r}})^{\text{T}}$. The wave equation (70) is coupled with the vorticity and entropy equations (71) and (72) via the right-hand side. Note that similar to the vorticity equation of the system, the entropy equation does not describe convection. Since the entropy equation (72) is stable, it can be concluded that the whole system remains stable, i.e., stability is also proven for the APE-2 system.

Note that for non-uniform mean flows in general the governing equation for the vorticity mode equation (67) and the wave equation (64) of the equivalent form of the linearized Euler equations are coupled. Hence, an alternative homogeneous scalar wave equation that is designed to describe wave propagation in a non-uniform mean flow without additional sources must also involve the description of vortex dynamics. The homogeneous Lilley equation [25] is the homogeneous scalar wave equation for a sheared mean flow that also possesses unstable solutions due to the encoded vortex dynamics. Dowling et al. [7] showed that a Green's function for the solution of the inhomogeneous wave equation related to a certain shear flow profile has to be weakly causal to suppress the occurrence of instabilities in the acoustic solution. The use of a

weakly causal Green's function can be deemed a way to suppress unstable vortex dynamics encoded in the wave equation. In [7] the choice of a weakly causal Green's function is stated to be physical since in a real flow the acoustic field does not depend solely on the unsteady near-field flow but rather is coupled such that acoustic waves are generated from turbulence which is partially caused by previously acoustically excited instabilities. Therefore, a theory that attributes the source of sound to the turbulence must allow for the sound's prior existence. Similarly the APE system can be understood as a system where the unstable governing equation for the vorticity mode equation (67) of the equivalent form of the LEE is modified to suppress the occurrence of instabilities while the governing acoustic equation (64) is retained and as such maintains a bounded solution. The weakly causal element comes into picture for the APE formulations via the acoustic source that has to be rigorously determined from a compressible initial flow simulation that also contains compressible, i.e., acoustic fluctuations in the source region.

3.5. APE variant 4

The last variant of acoustic perturbation equations is termed APE-4. It is derived by rewriting the governing flow equations such that the left-hand side is given by the APE-1 system derived in the Section 3.1 while the right-hand source side is defined by the remaining terms. The purpose is to find sources q_c and $\boldsymbol{q}_m$ of the APE-1 system (47) and (48) that can be easily computed from a compressible flow simulation without solving a Poisson equation. Although such sources will excite also vorticity disturbances in the APE-1 system, stability is not affected as discussed in Section 3.4. As shown below the vortex sound source is based on the Lamb vector $\boldsymbol{L} = \boldsymbol{\omega} \times \boldsymbol{u}$, i.e., the vorticity based source term of the acoustic analogies of Powell [33], Howe [20] and Möhring [27,28]. The Lamb vector will vanish close to solid boundaries due to the no-slip condition, where the flow simulation generally requires the highest resolution. Hence, the acoustic grid can be coarser than the fluid mechanical grid to properly resolve the acoustic sources. Furthermore, since the APE systems do not describe convection of vortical or entropy disturbances, no CFL restrictions related to non-acoustic modes limit the time step.

In the following the continuity and Navier–Stokes equations are written in primitive non-linear disturbance formulation. To obtain a system with the perturbation pressure as variable the second law of thermodynamics in the first-order formulation is used. The non-linear terms containing entropy fluctuations are dropped for convenience. These neglected terms just occur as additional source terms on the right-hand side of the final formulation. The governing equations can be written as

$$\frac{\partial \rho'}{\partial t} + \nabla \cdot \left(\bar{\rho}\boldsymbol{u}' + \rho'\bar{\boldsymbol{u}} + \rho'\boldsymbol{u}' - \overline{\rho'\boldsymbol{u}'} \right) = 0, \tag{73}$$

$$\frac{\partial \boldsymbol{u}'}{\partial t} + \left(\bar{\boldsymbol{u}} \cdot \nabla \right)\boldsymbol{u}' + \left(\boldsymbol{u}' \cdot \nabla \right)\bar{\boldsymbol{u}} + \nabla\left(\frac{p'}{\bar{\rho}} \right) = \boldsymbol{f}_{\text{nonlinear}} + \boldsymbol{f} \tag{74}$$

with the momentum sources

$$\boldsymbol{f}_{\text{nonlinear}} = -\left(\left(\boldsymbol{u}' \cdot \nabla \right)\boldsymbol{u}' - \frac{\nabla \cdot \underline{\boldsymbol{\tau}}}{\rho} \right)' \quad \text{and} \quad \boldsymbol{f} = T'\nabla\bar{s} - s'\nabla\bar{T},$$

where the perturbation density is connected to the perturbation pressure via Eq. (46). Primed quantities denote perturbation variables, while time-averaged values are denoted by a bar. To derive the particular form of Eq. (74) the enthalpy and entropy gradients are substituted for the pressure gradient in the full non-linear momentum equation using the second law of thermodynamics equation (26). The equations for the perturbation quantities follow by subtracting the time-averaged momentum equation. Since differentiation and time averaging can be exchanged, only the gradient of the perturbation enthalpy $\nabla h' = \nabla h - \overline{\nabla h}$

remains in the momentum equation. Furthermore, subtraction of the time-averaged Euler equations yields for the entropy gradients $T\nabla s - \overline{T\nabla s} \approx \bar{T}\nabla s' + T'\nabla\bar{s}$. Finally, the first-order formulation of the second law of thermodynamics equation (44) is substituted for the perturbation enthalpy h'. Now, using the identity

$$\left(\bar{\boldsymbol{u}}\cdot\nabla\right)\boldsymbol{u}' + \left(\boldsymbol{u}'\cdot\nabla\right)\bar{\boldsymbol{u}} = \nabla\left(\bar{\boldsymbol{u}}\cdot\boldsymbol{u}'\right) + \boldsymbol{\omega}'\times\bar{\boldsymbol{u}} + \bar{\omega}\times\boldsymbol{u}'$$

the structure of the left-hand side corresponds to the APE-1 system

$$\frac{\partial p'}{\partial t} + \bar{c}^2\nabla\cdot\left(\bar{\rho}\boldsymbol{u}' + \bar{\boldsymbol{u}}\frac{p'}{\bar{c}^2}\right) = \bar{c}^2 q_c, \tag{75}$$

$$\frac{\partial \boldsymbol{u}'}{\partial t} + \nabla\left(\bar{\boldsymbol{u}}\cdot\boldsymbol{u}'\right) + \nabla\left(\frac{p'}{\bar{\rho}}\right) = \boldsymbol{q}_m, \tag{76}$$

while the right-hand side sources read

$$q_c = -\nabla\cdot\left(\rho'\boldsymbol{u}'\right)' + \frac{\bar{\rho}}{c_{\mathrm{p}}}\frac{\bar{D}s'}{Dt}, \tag{77}$$

$$\boldsymbol{q}_m = -(\boldsymbol{\omega}\times\boldsymbol{u})' + T'\nabla\bar{s} - s'\nabla\bar{T} - \left(\nabla\frac{(u')^2}{2}\right)' + \left(\frac{\nabla\cdot\underline{\tau}}{\rho}\right)'. \tag{78}$$

Eqs. (75) and (76) with sources (77) and (78) constitute the APE-4 system. In [29] an acoustic analogy is defined to be any 'noise theory in which the equations of motion for a compressible fluid are rearranged in a way that separates linear propagation effects.' Since the linear APE system plus the above sources follow from the governing flow equations, where the major linear source terms are expressions in vorticity and entropy in the sense of the above definition, this system constitutes an acoustic analogy in which sound is generated by vorticity and entropy inhomogeneities.

As usual whenever acoustic analogies are applied, the viscous terms in the source are assumed to be of negligible importance. Furthermore, as evidenced in Section 4.4 the non-linear and entropy terms are of minor importance considering vortex sound problems. Then, the major vortex source term is the Lamb vector, i.e., $\boldsymbol{q}_m = -\boldsymbol{L}' = -(\boldsymbol{\omega}\times\boldsymbol{u})'$.

4. Computational results

4.1. Numerical method

The acoustic perturbation equations (APEs) and the linearized Euler equations (LEEs) can be written in non-dimensional form including a source term $\boldsymbol{S}$ in generalized curvilinear coordinates (ξ_1, ξ_2)

$$\frac{\partial \boldsymbol{U}}{\partial t} + \hat{\boldsymbol{A}}_i\frac{\partial \boldsymbol{U}}{\partial \xi_i} + \boldsymbol{H}\cdot\boldsymbol{U} = \boldsymbol{S} \quad \text{with } \hat{\boldsymbol{A}}_i = \boldsymbol{A}_j\frac{\partial \xi_i}{\partial x_j}, \tag{79}$$

where $\boldsymbol{U}$ is the vector of the primitive perturbation variables. The Jacobian matrix $\boldsymbol{A}_j$ and the matrix $\boldsymbol{H}$, that contains all the mean flow gradients, follow from the particular form of the linearized equations. The equations are non-dimensionalized by an appropriate reference length, the sound speed c_∞, and the density

ρ_∞ of the freestream. The pressure and timescale are non-dimensionalized with l/c_∞ and $\rho_\infty c_\infty^2$. Einstein's summation convention is to be applied to the products with equal indices.

For the spatial discretization the fourth-order dispersion relation preserving (DRP) scheme of Tam and Webb [40] is applied. This scheme is designed such that for a wide range of wave numbers the dispersion relations of the LEE are preserved.

The temporal integration is performed with the fourth-order alternating two-step low-dissipation and low-dispersion Runge–Kutta scheme (LDDRK 5-6) proposed by Hu [21]. Thus, the numerical method is fourth-order accurate in space and time. To suppress spurious high frequency waves artificial selective damping (ASD) according to Tam and Dong [38] is used. A constant background value of the mesh Reynolds number with a typical value of $1/Re_\Delta = 0.05$ with a slight increase close to boundaries is used. Besides artificial selective damping also explicit commutative filters according to Vasilyev et al. [41] are used. A simple sponge layer boundary conditions is applied at far-field boundaries [11].

The formulation of the solid wall boundary conditions is based on the ghost-point concept proposed by Tam and Dong [39]. In this ansatz a biased finite difference stencil, which includes the ghost-point below the wall, is used. The value of the pressure of the ghost-point is determined such that the wall normal pressure derivative satisfies the boundary condition, e.g.,

$$\frac{\partial p'}{\partial n} = 0. \tag{80}$$

For flows over slightly curved surfaces it follows from the linearized Euler equations that the kinematic boundary condition

$$\boldsymbol{u}' \cdot \boldsymbol{n} = 0 \tag{81}$$

is automatically satisfied if the normal pressure derivative vanishes. For the APE-1 system the pressure boundary condition is also defined by Eq. (80). For the APE-2 system the decomposition in Eq. (52) means to split the perturbation pressure further into one part, which is interpreted as pseudosound, and the remaining contribution p^{a}. Hence, for the variable p^{a} of the APE-2 system the boundary condition becomes

$$\frac{\partial p^{\mathrm{a}}}{\partial n} = -\frac{\partial \bar{\rho} \Phi_{\mathrm{P}}}{\partial n}.$$

In the APE-1 and the APE-2 formulation the pressure conditions at the boundary are satisfied in conjunction with the ghost-point concept.

Note that the velocity variable $\boldsymbol{u}^{\mathrm{a}}$ of the APE-1 and APE-2 system excludes the solenoidal perturbation velocity $\boldsymbol{u}^{\mathrm{v}}$ and as such the resulting velocities do not obey the kinematic boundary condition, i.e.,

$$\boldsymbol{u}^{\mathrm{a}} \cdot \boldsymbol{n} = -\boldsymbol{u}^{\mathrm{v}} \cdot \boldsymbol{n} \neq 0.$$

In other words, the boundary condition based on the ghost-point concept yields for these cases a general non-vanishing velocity normal to the surface. However, for the APE-4 formulation, that uses the perturbation velocity $\boldsymbol{u}'$ as variable, the kinematic boundary condition (81) holds, since vortical perturbations are not excluded from the perturbation velocities. Furthermore, the perturbation pressure is not split for the APE-4 formulation. Hence, the normal derivative at the wall can be prescribed for weakly curved surfaces by Eq. (80).

4.2. Wave propagation in a sheared mean flow

Since the homogeneous acoustic perturbation equations describe properly the wave propagation for irrotational mean flows, an error occurs applying the homogeneous APE systems in mean flows with

vorticity. For example in the APE-1 system the acoustic source, which arises from the propagation of acoustic perturbations in a mean flow with vorticity, i.e., term IV in Eq. (48), is dropped. However, it is clear that the error made in neglecting the acoustic source term IV is much smaller than neglecting any acoustic convection and refraction at all, e.g., by applying Lighthill's acoustic analogy with an artificially truncated source region.

To quantify the error made by neglecting the secondary acoustic sources the sound field generated by an analytically prescribed monopole source in a mean flow with vorticity is computed with the APE-2 systems and is juxtaposed to the solution obtained with the linearized Euler equations and the same source as governing acoustic equations. The test problem is a sheared mean flow whose velocity distribution is illustrated in Fig. 2. Since the thickness of the shear layer remains constant, no instability waves are excited in the LEE. The mean velocity profile is prescribed analytically by

$$u(y) = \Delta u \tanh(2y/\delta_\omega), \tag{82}$$

where the peak velocity is set to $\Delta u = 0.5 c_\infty$. Note that the wave operator encoded in all APE formulations is valid for arbitrary mean flows, i.e., is not restricted to low Mach number flows. A low Mach number limitation appears only via the simplified source IIIb (Eq. (56)) in the APE-2 system. However, in this test problem the APE-2 system is excited by an analytically prescribed monopole source, that appears on the right-hand side of the continuity equation.

The shear-layer thickness is fixed by the parameter δ_ω. Its value is either $\delta_\omega = 50$ or $\delta_\omega = 10$, since a smaller thickness causes higher values of the mean flow vorticity and as such larger errors in the wave propagation will occur.

The non-dimensional mean density is defined to be constant, i.e., $\overline{\rho} = 1$. A computational domain with 201×201 points and equidistant grid spacing $\Delta x = \Delta y = 1$ ranging from -100 to 100 in both directions is used. The reference solution is based on the linearized Euler equations:

$$\frac{\partial \rho'}{\partial t} + \nabla \cdot \left(\rho' \bar{\boldsymbol{u}} + \bar{\rho} \boldsymbol{u}' \right) = q_c, \tag{83}$$

$$\frac{\partial \boldsymbol{u}'}{\partial t} + \left(\bar{\boldsymbol{u}} \cdot \nabla \right) \boldsymbol{u}' + \left(\boldsymbol{u}' \cdot \nabla \right) \bar{\boldsymbol{u}} + \frac{\rho'}{\bar{\rho}} \left(\bar{\boldsymbol{u}} \cdot \nabla \right) \bar{\boldsymbol{u}} + \frac{\nabla p'}{\bar{\rho}} = \boldsymbol{q}_m, \tag{84}$$

$$\frac{\partial p'}{\partial t} - \bar{c}^2 \frac{\partial \rho'}{\partial t} = q_e. \tag{85}$$

In this particular form the energy equation follows from the first-order Eq. (46). The APE-2 and the LEE system are excited by an analytically prescribed monopole source of the continuity equation

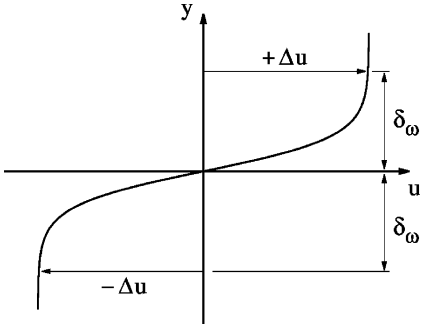

Fig. 2. Sketch of the sheared mean flow with a zero convection velocity at $y = 0$. The peak velocity is $\Delta u = 0.5 c_\infty$.

$$q_c = \exp\left[-\ln(2)\frac{x^2+y^2}{\sigma^2}\right]\cdot\cos(\omega t), \tag{86}$$

with $\sigma^2 = 9$ and an angular frequency $\omega = 0.5$. The source is located in the origin of the computational domain. No other sources are considered neither in the LEE nor in the APE-2 formulation. Fig. 3 shows a snapshot of the perturbation pressure from the solution of the linearized Euler equation and the APE-2 system, respectively, for a layer thickness $\delta_\omega = 50$. The agreement is perfect. This result is confirmed by comparing the pressure distributions on the line $y = 70$. Fig. 4 shows distributions of the acoustic pressure and its RMS value. The curves of the LEE and the APE-2 solutions match very well. The solution of the pressure distribution for a shear layer parameter $\delta_\omega = 10$ is evidenced in Fig. 5. Even an approx. five times larger mean vorticity causes only small differences between the predicted pressure levels. Thus, we conclude that the homogeneous APE system is appropriate to describe wave propagation in arbitrary mean flows with sufficiently small levels of mean vorticity.

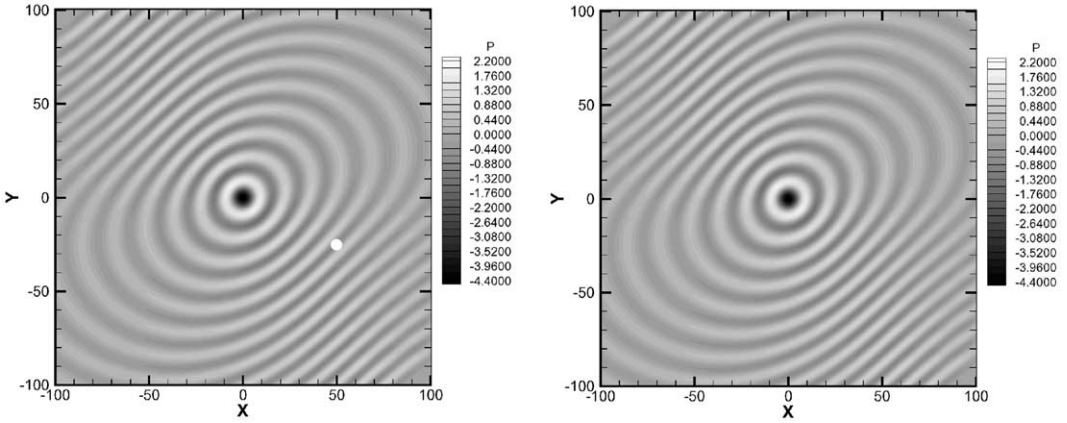

Fig. 3. Snapshot of the pressure contours resulting from a monopole in sheared mean flow, $\delta_\omega = 50$, time level $T = 180$. Solutions of the linearized Euler equations (left) and the acoustic perturbation equations (APE-2) (right).

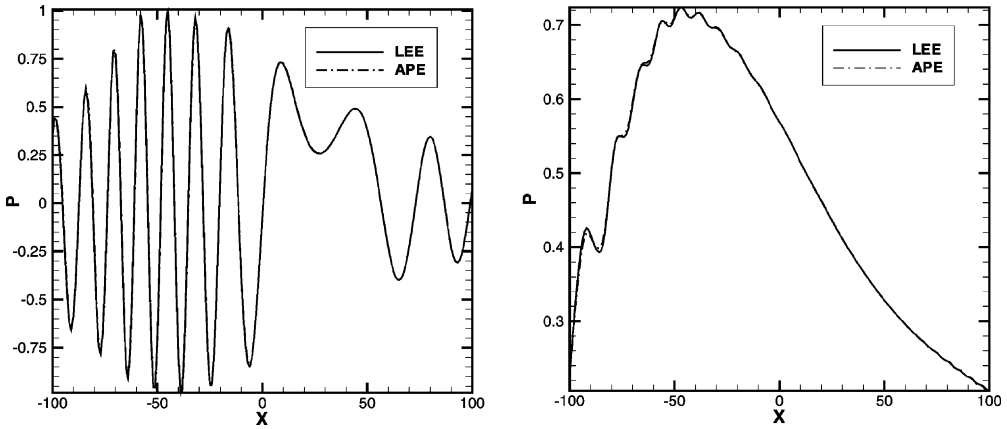

Fig. 4. Comparison of the acoustic pressure distribution along line $y = 70$ for the linearized Euler equations and the APE-2 system. Shear layer thickness $\delta_\omega = 50$. Pressure distribution at $T = 180$ (left) and distribution of RMS pressure (right).

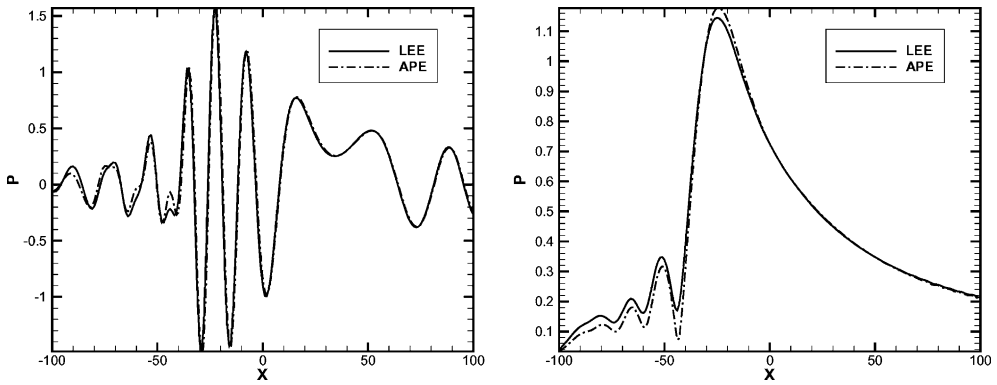

Fig. 5. Comparison of the acoustic pressure distribution along line $y = 70$ for the linearized Euler equations and the APE-2 system. Shear layer thickness $\delta_\omega = 10$. Pressure distribution at $T = 180$ (left) and distribution of RMS pressure (right).

4.3. Sound generation of a spinning vortex pair

In order to numerically study the capabilities of the various APE formulations to predict acoustic fields based on prescribed sources the sound generation due to a spinning vortex pair is considered next. The spinning vortex pair has been computed, e.g., in the work of Lee et al. [22], Ekaterinaris [8], and Slimon et al. [37], to evaluate the capability of the acoustic/viscous splitting technique proposed by Hardin and Pope [16] and some derivatives of it to predict its quadrupolar sound field. Fig. 6 shows a sketch of the flow configuration. The flow field induced by a spinning vortex pair is assumed inviscid and incompressible. The two-point vortices are separated by a distance of $2r_0$ and have a circulation Γ. The rotation period is $T = 8\pi^2 r_0^2/\Gamma$, the angular velocity is given by $\omega = \Gamma/4\pi r_0^2$, and the circumferential Mach number is $M_r = \Gamma/4\pi r_0 c_\infty$. Müller and Obermeier give in [30] an analytical solution of the induced acoustic field, which is based on a matched asymptotic expansion (MAE) of the flow problem. The inner solution is inferred from the incompressible and inviscid flow problem. The flow field of a pair of vortices is determined by the complex potential function $\Phi(z, t)$

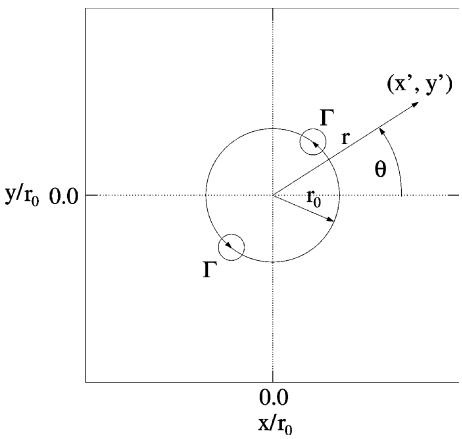

Fig. 6. Sketch of the spinning vortex pair. The distance between both vortices is $2r_0$.

$$\Phi(z,t) = \frac{\Gamma}{2\pi \mathrm{i}} \ln z^2 \left(1 - \frac{b^2}{z^2}\right) \approx \frac{\Gamma}{\pi \mathrm{i}} \ln z - \frac{\Gamma}{2\pi \mathrm{i}} \left(\frac{b}{z}\right)^2 = \Phi_0 + \Phi_1, \tag{87}$$

where $z = r\mathrm{e}^{\mathrm{i}\theta} = x' + \mathrm{i}y'$ and $b = r_0 \mathrm{e}^{\mathrm{i}\omega t}$. The potential Φ in Eq. (87) is split into a steady vortical flow part Φ_0 and the first leading term Φ_1 of the expansion of the unsteady flow part for $|z/b| \gg 1$. Due to the exponent 2 the leading unsteady part describes a fluctuating field with angular frequency 2ω. The outer acoustic field is prescribed by the homogenous wave equation. Matching between outer and inner solution yields a solution for the outer acoustic potential which leads to

$$\widetilde{p}' = \frac{\rho_\infty \Gamma^4}{64\pi^3 r_0^4 c_\infty^2} H_2^{(2)}(kr), \tag{88}$$

whose real part represents the pressure fluctuation and $H_2^{(2)}(kr)$ denotes the Hankel function of second order and second kind. The wave number is $k = 2\omega/c_\infty$. The incompressible velocity and the incompressible perturbation pressure are determined by the complex potential Φ via

$$U - \mathrm{i}V = \frac{\partial \Phi(z,t)}{\partial z}, \quad P' = -\rho_\infty \left[\frac{\partial}{\partial t} \Re\{\Phi(z,t)\} + \frac{1}{2}\left(U^2 + V^2\right)\right]. \tag{89}$$

The incompressible perturbation pressure is used to compute the source term IIIb (Eq. (56)) of the APE-2 system (53) and (55). In the APE-4 system (75) and (76) the vortex source term based on the Lamb vector $\boldsymbol{\omega} \times \boldsymbol{u}$ is determined. Since the vorticity of the flow problem in Fig. 6 is confined to δ-functions, the point-like vortices are approximated using a vortex core model based on a Gaussian vorticity distribution with a standard deviation $\sigma \approx r_0$ such that the source becomes

$$\boldsymbol{q}_m(\boldsymbol{r},t) = -\frac{\Gamma^2 \boldsymbol{e}_r(t)}{8\pi^2 \sigma^2 r_0} \sum_{i=1}^{2} (-1)^i \exp\left(-\frac{|\boldsymbol{r} + (-1)^i \boldsymbol{r}_0(t)|^2}{2\sigma^2}\right), \quad \sigma \approx r_0$$

with $\boldsymbol{r} = (x,y)^{\mathrm{T}}$, $\boldsymbol{r}_0 = r_o \boldsymbol{e}_r$, and $\boldsymbol{e}_r = (\cos\theta, \sin\theta)^{\mathrm{T}}$, $\theta = \omega t$. The computational domain has an extension of $-100 \leqslant x/r_0 \leqslant 100$ in the x- and y-direction. The interior grid consists of 141×141 points with a surrounding sponge layer thickness of 11 points. In order to resolve the vortex source properly the orthogonal grid is clustered close to the origin. Spurious waves are removed using spatial filtering. Fig. 7 evidences

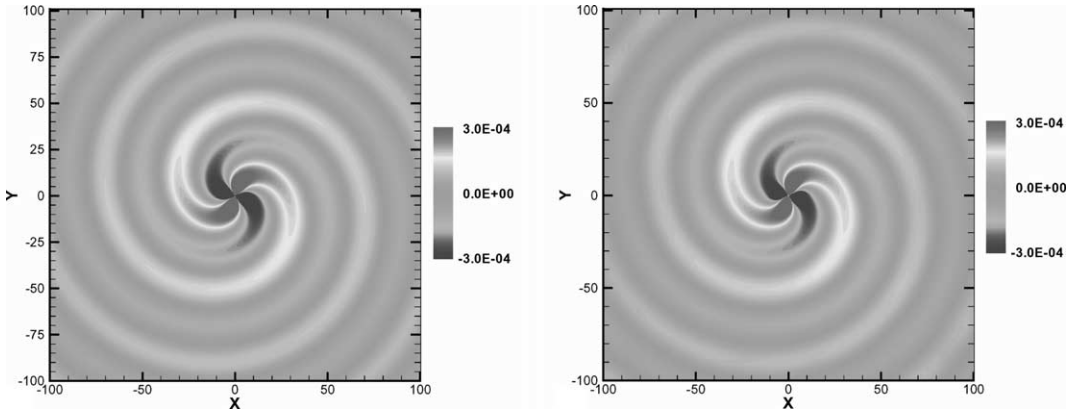

Fig. 7. Comparison of the acoustic pressure contours for a matched asymptotic expansion (MAE) solution (left) and the solution of the APE-4 system with vortex source term (right). $\Gamma/(c_\infty r_0) = 1.0$, $M_r = 0.0796$.

good agreement of the pressure contours of the MAE solution and the solution of the APE-4 system. Figs. 8 and 9 show a comparison of the pressure distribution along the diagonal $x = y$ of the MAE solution with the solutions of the APE-2 and APE-4 systems for three different vortex circulations and spinning frequencies, i.e., $\Gamma/(c_\infty r_0) = 0.6, 1.0, 1.6$. At the origin of the computational domain, i.e., midway between the two point vortices, the incompressible pressure becomes singular and its value is very large close to the vortex centers. In this region the velocity and pressure distributions have large gradients. While the acoustic source of the APE-4 system is computed using a vortex core model, the acoustic source of the APE-2 system, i.e., the time derivative of the incompressible pressure (Eq. (89)) is determined only for grid points with a distance $r/r_0 \geqslant 2.0$ from the origin. As discussed in [8] this procedure avoids the generation of spurious waves.

Overall the acoustic fields of the APE formulations show good agreement with the analytical solution for all frequencies. Probably due to the truncated incompressible pressure source of the APE-2 system the pressure distributions show a small shift relative to the MAE reference solution and deviate close to the origin in Figs. 8 and 9. The solutions based on the APE-4 system with vortex source match very well the

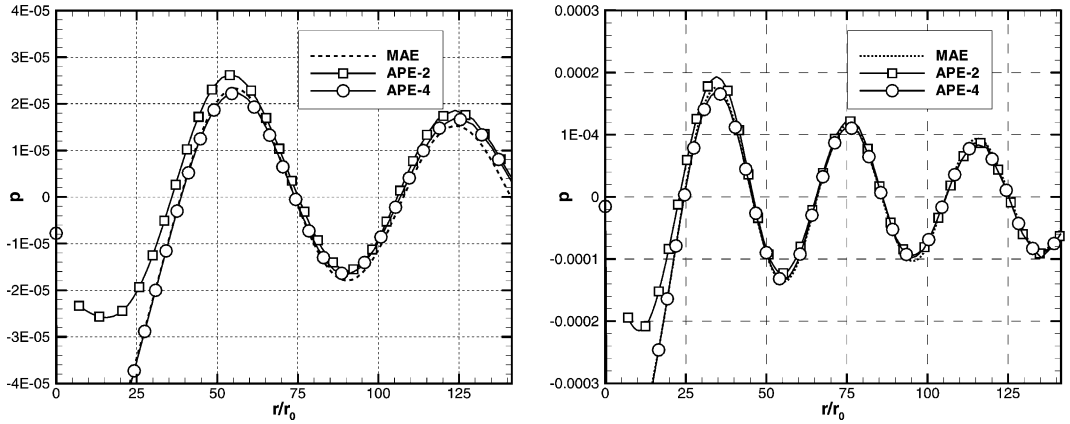

Fig. 8. Comparison of the acoustic pressure distribution along the diagonal line $x = y$ for the matched asymptotic expansion (MAE) solution and solutions of the APE-2 and APE-4 systems. $\Gamma/(c_\infty r_0) = 0.6$, $M_r = 0.0477$ (left) and $\Gamma/(c_\infty r_0) = 1.0$, $M_r = 0.0796$ (right).

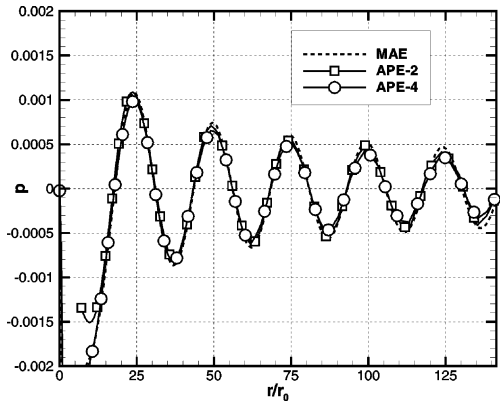

Fig. 9. Comparison of the acoustic pressure distribution along the diagonal line $x = y$ for the matched asymptotic expansion (MAE) solution and solutions of the APE-2 and APE-4 systems. $\Gamma/(c_\infty r_0) = 1.6$, $M_r = 0.1273$.

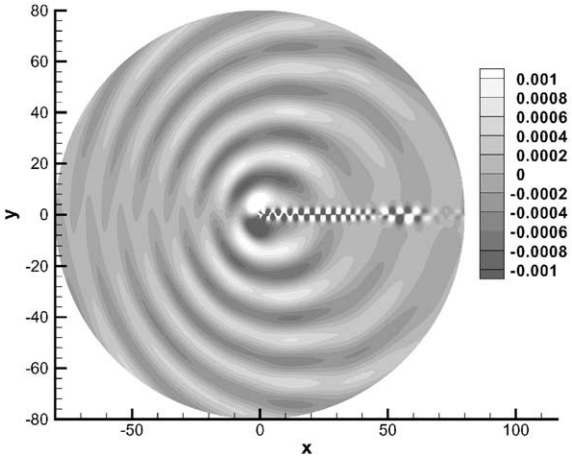

Fig. 10. Perturbation pressure contours p' of a highly resolved unsteady flow simulation, $Re = 200$, $M = 0.3$.

reference solution. Close to the outer boundaries small deviations between the computed and the analytical solution occur in Figs. 8 and 9 due to the sponge layer boundary condition.

4.4. Cylinder in a crossflow

The flow around a circular cylinder at Mach number $M = 0.3$ and Reynolds number $Re = 200$ is used as a further test problem to compare the prediction quality of the APE-2 and APE-4 formulations with the direct numerical simulation. The compressible flow simulation is carried out using a second-order AUSM scheme for the spatial discretization. An O-grid with a radial extension of $r/d = 80$ cylinder diameters and a resolution of 657×513 grid points in the circumferential and the radial direction, respectively, is used for the flow computation. Fig. 10 shows the perturbation pressure field $p' = p - \bar{p}$ obtained from the CFD simulation.

The acoustic computations are performed on an O-grid with 257×161 grid points in the circumferential and radial directions. The acoustic sources are computed from the CFD solution using second-order schemes. One time period of the vortex shedding, non-dimensionalized with the cylinder diameter d and the far-field sonic speed c_∞, is $T = 17$. From the time period the non-dimensional wave length is $\lambda/d = 17$ such that the coarsest resolution on the CFD grid at the outer boundary in the circumferential direction comprises about 22 points per wave length (PPW), which is the resolution limit for a second-order central finite difference scheme. The lowest acoustic resolution is about 8.6 PPW, which is slightly higher than the theoretical resolution limit 5.4 PPW of the DRP-scheme. The time period is split into 43 source time levels and during the acoustic simulation the time-dependent source is computed by linearly interpolating between two adjacent source data time levels. Due to the periodicity of the flow problem a long time integration source is obtained by repeatedly reading the single source data period. The acoustic simulation is performed for several equation sets, i.e., LEE, APE-2, and APE-4, and various source term formulations, which are given in Table 1 [2]. The linearized Euler equations (83)–(85) are used with a source

[2] Note that the extension of the CFD simulation allows to compute the sources in the whole acoustic domain. According to Fig. 1 the hybrid approach in general gives the source just in a reduced domain, hence interior boundaries appear where the source must be truncated in the wake behind the body. It was demonstrated in [9] that spurious sound due to the truncated source can be suppressed effectively, e.g., by either damping the source term or applying analytical corrections.

Table 1
Description of the acoustic equations and sources

Case	Acoustic equation	Source
A	LEE	$-\partial p/\partial t$ from compressible CFD
B	APE-2	$-\partial p/\partial t$ from compressible CFD, spatial filtering equation (90) with $\sigma = 5$
C	APE-2	$-\partial p/\partial t$ from compressible CFD, spatial filtering equation (90) with $\sigma = 20$
D	APE-2	$-\bar{\rho}\partial\Phi_{\mathrm{P}}/\partial t$, Eq. (38)
E	APE-4	$-(\boldsymbol{\omega}\times\boldsymbol{u})'$

$$q_c = 0, \quad \boldsymbol{q}_m = \mathbf{0}, \quad q_e = -\frac{\partial P'}{\partial t}.$$

This particular source follows by linearizing the acoustic equations proposed by Shen et al. [35].

Fig. 11 shows pressure contours and the pressure distribution on $x = 0$ for the LEE simulation. The pressure contour levels evidence the perturbation pressure levels to be overpredicted by a factor 3 compared to the highly resolved CFD simulation (Fig. 10). The time dependence of the perturbation pressure in a receiving point $r/d = 40$ diameters above the cylinder indicates that the LEE simulation becomes unstable for $T > 200$. The globally unstable mean flow around the cylinder leads to a divergence of the LEE simulation due to excited hydrodynamic instabilities, which are not limited neither by non-linear saturation nor viscous damping.

Since the acoustic perturbation equations are stable for arbitrary mean flow fields, as is shown in Sections 3.4 and 3.5, the APE-2 system is applied to this test problem to investigate numerically this theoretical result. Furthermore, it is checked whether the perturbation pressure of the $M = 0.3$ compressible flow simulation can be used instead of that of an incompressible solution to express the source IIIb. In this case errors can occur since the source based on the pressure time derivative will contain an additional compressible, i.e., acoustic, contribution that will generate non-physical signals. Although the magnitude of the compressible fluctuations in the source is small, they decay very slowly. Hence, this contribution might have a considerable influence on the predicted acoustic pressure magnitudes. To separate the essential hydrodynamic near field from the acoustic far field the time derivative of the compressible perturbation pressure is spatially filtered using a Gaussian shape filter with origin in the cylinder center and a filter width determined by the parameter σ, i.e.,

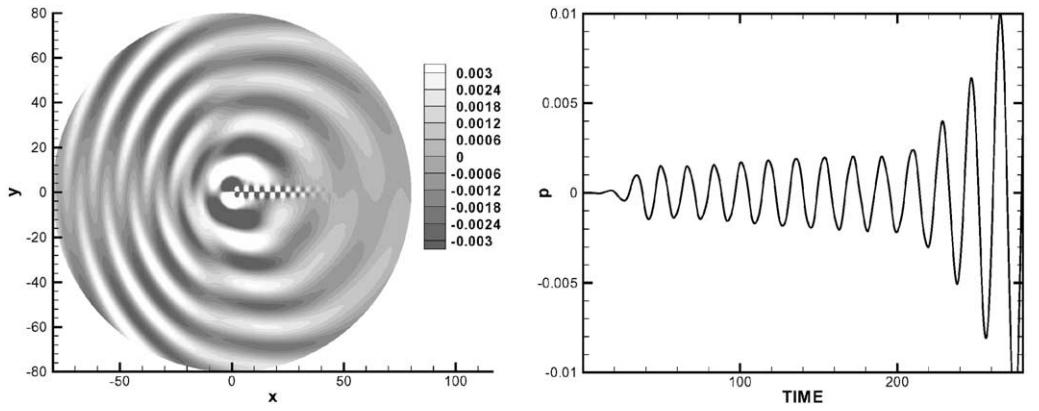

Fig. 11. Case A, Table 1: Perturbation pressure contours from a solution of the linearized Euler equations (LEE) with source term Eq. (85), i.e., pressure time derivative from the CFD solution at time $T = 200$ (left). The perturbation pressure level exceeds that of the CFD solution by a factor 3. Unstable perturbation pressure signal of the LEE simulation for a point $r/d = 40$ above the cylinder for $T > 200$ (right).

$$\frac{\partial}{\partial t}\bar{\rho}\Phi_{\mathrm{P}} \approx \left\langle \frac{\partial p}{\partial t} \right\rangle = \frac{\partial p}{\partial t} \exp\left(-\frac{(r-r_0)^2}{\sigma^2} \right). \tag{90}$$

Fig. 12 shows pressure contours for two different spatial filters. Due to the APE-2 formulation the hydrodynamic perturbation pressure is excluded from the perturbation pressure. Hence, no vortex street is visible in the simulation. The filter width $\sigma = 20$ causes the acoustic pressure to be too large compared to the reference solution in Fig. 10. For a small filter width $\sigma = 5$ the magnitude of the acoustic pressure and the lobes tilted in the flow direction agree fairly well with the CFD solution. Nevertheless, this result indicates an inappropriate sensitivity of the simulation to the filter width. It must be emphasized, however, that the simulation using the APE-2 system confirms the stability analysis in Section 3.4, since no unstable behavior occurs during the non-dimensional time period $\Delta T \approx 600$. Furthermore, Fig. 13 evidences the

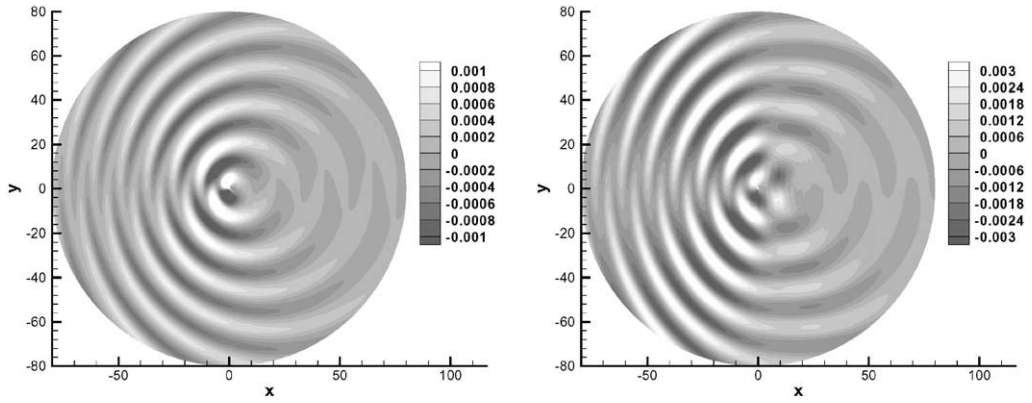

Fig. 12. Case B, C, Table 1: Acoustic pressure contours from the APE-2 solution with spatially filtered pressure time derivative from the CFD solution as source. $\sigma = 5$ (left), $\sigma = 20$ (right).

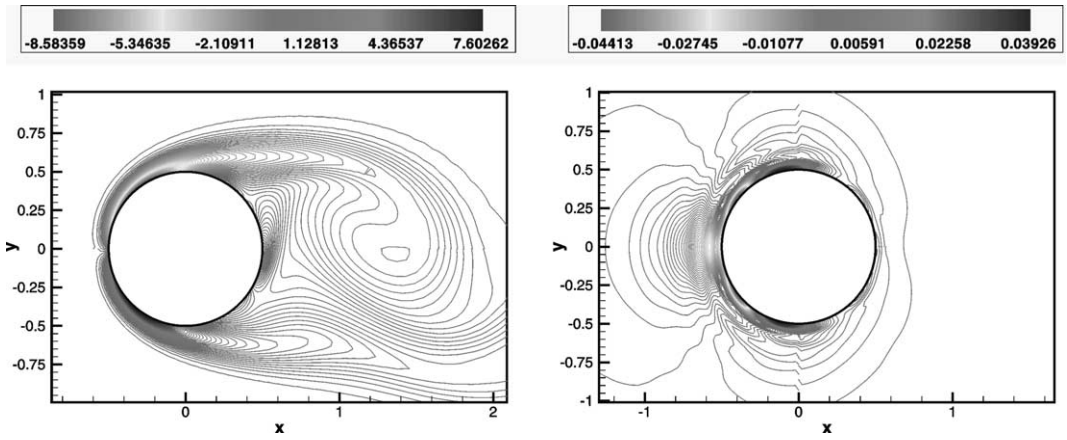

Fig. 13. Comparison of the perturbation vorticity levels $\boldsymbol{\omega}' = \nabla \times \boldsymbol{u}'$ of the CFD solution (left) with the perturbation vorticity in the acoustic simulation of the APE-2 system (Case B, Table 1) (right). The levels of the acoustic simulation evidence that only a small amount of vorticity is generated due to the wall boundary condition. Hence, the integrability condition $\nabla \times \boldsymbol{u}^{\mathrm{a}}$ is supported by the numerical scheme.

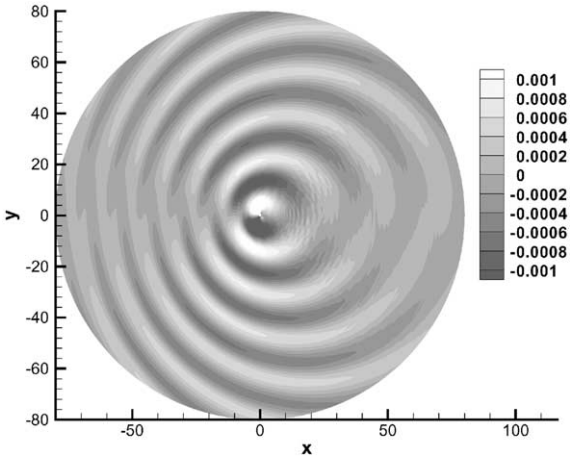

Fig. 14. Case D, Table 1: Perturbation pressure contours of the APE-2 formulation using the vortex source from the unsteady flow simulation, $Re = 200$, $M = 0.3$.

excitation of vortical disturbances to be strongly suppressed. For the APE-2 system (Case B) a non-zero modulus of the perturbation vorticity appears only close to the boundary, which is, compared to the perturbed vorticity levels of the unsteady flow field, strongly reduced such that the integrability condition $\nabla \times \boldsymbol{u}^{\mathrm{a}}$ inherent in the APE-formulation is supported by the numerical scheme except for the small error due to the solid-wall boundary condition.

To obtain an appropriate source IIIb of the APE-2 system from a compressible flow simulation, Eq. (38) has to be properly solved for Φ_{P}. This is achieved by computing the solenoidal perturbation velocity

$$\boldsymbol{u}^{\mathrm{v}} = \left(\frac{\partial \Psi}{\partial y}, -\frac{\partial \Psi}{\partial x} \right)^{\mathrm{T}}$$

in an intermediate step by solving a Poisson problem for a streamfunction Ψ

$$\nabla^2 \Psi = -\omega'.$$

The boundary conditions are the Dirichlet condition $\Psi = u_\infty y$ at the far-field boundaries and the Neumann condition $\partial \Psi / \partial n = 0$ at the cylinder surface. The latter constitutes the no-slip condition at the surface, which holds approximately for the solenoidal velocity decomposition at small Mach numbers. Eq. (38) is solved by dropping the viscous terms, since the double divergence of the stress tensor vanishes for low Mach number flows. Then, Eq. (38) corresponds to the (perturbed) pressure Poisson equation used in the framework of incompressible flow solver algorithms. [3]

Fig. 14 shows the solution for source Φ_{P} (Case D). The pressure magnitudes agree fairly well with those of the CFD reference solution in Fig. 10.

Fig. 15 shows the perturbation pressure field obtained from the APE-4 system (Eqs. (75) and (76)) using the vortex source $(\boldsymbol{\omega} \times \boldsymbol{u})'$. According to the formulation of the acoustic perturbation equations a vortex street occurs in the simulation since the hydrodynamic pressure fluctuations are included in the pressure. The pressure magnitudes and the shape of the radiated waves agree well with those of the CFD simulation

[3] Of course, it would be most appropriate to determine the source term IIIb via a solution of the incompressible flow using Eq. (56). However, based on a compressible flow simulation the above-mentioned strategy is to be followed.

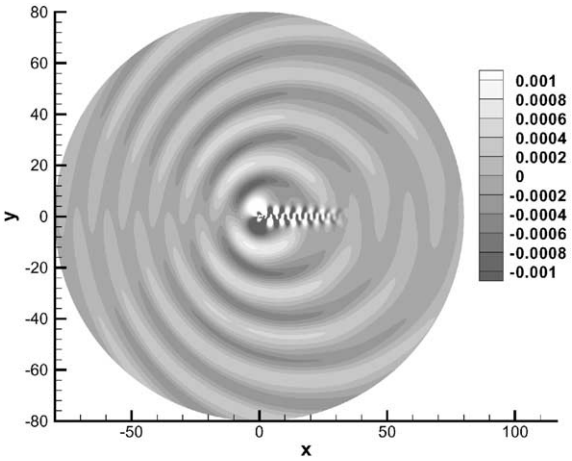

Fig. 15. Case E, Table 1: Perturbation pressure contours of the APE-4 formulation using the vortex source from the unsteady flow simulation, $Re = 200$, $M = 0.3$.

in Fig. 10. Due to the mean flow the two main lobes in the upper and lower half plane are tilted in the upstream direction.

The decay of RMS pressure distributions of the APE-2 and APE-4 simulation is depicted in Fig. 16. On the left-hand side snapshots of the perturbation pressure distributions along a vertical line $x = 0$ are shown for the highly resolved CFD simulation and for the simulations based on the APE-2 and APE-4 formulations. The APE predictions differ on a 8 times coarser grid less than 1 dB relatively to the reference solution. The APE-4 solution is based (i) on a source term including besides the viscous term all linear and non-linear contributions and (ii) on a source term using the Lamb vector $(\boldsymbol{\omega} \times \boldsymbol{u})'$. The solutions evidence the latter to be the most important vortex sound source, since the entropy and non-linear terms show nearly no influence on the result. On the right-hand side the decay of the RMS pressure is plotted along the vertical line $x = 0$. In the near-field close to the vicinity of the cylinder the pressure waves show a decay

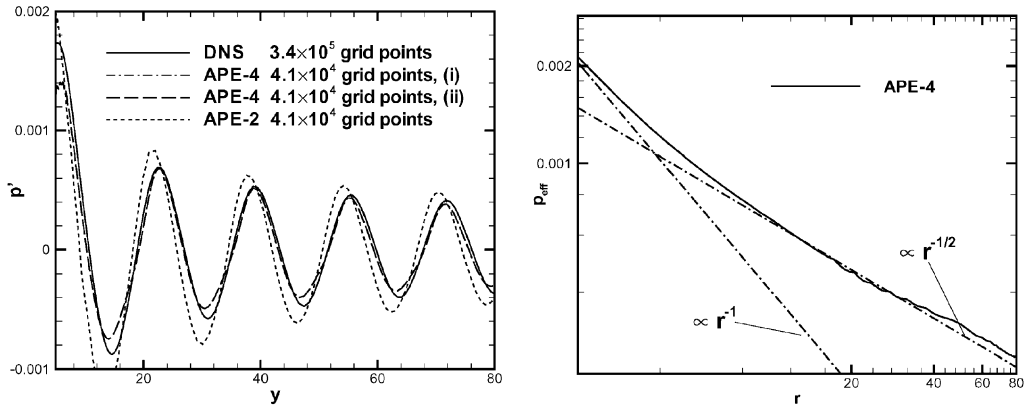

Fig. 16. Perturbation pressure distribution along a line $x = 0$ perpendicular to the mean flow direction for the DNS, APE-4 (i) with source including entropy and non-linear source terms, (ii) with Lamb vector $\boldsymbol{L}' = (\boldsymbol{\omega} \times \boldsymbol{u})'$ alone, and APE-2 solution case D, Table 1. Decay of the sound pressure perpendicular to the mean flow direction, APE-4 solution (right).

$\propto r^{-1}$. The acoustic waves confirm a decay with $r^{-1/2}$ towards the far field, which is in agreement with the asymptotic 2D behavior.

5. Conclusions

For a hybrid approach a family of acoustic perturbation equations (APEs) has been derived for the simulation of acoustic fields in space and time. The acoustic sources are predicted based on an unsteady flow simulation. Since the acoustic perturbation equations describe mean flow convection effects, the flow simulation has to comprise only the significant source region. It is shown analytically that the APE formulations do not possess instabilities for any non-uniform mean flow field with arbitrary density gradients. Several source term formulations have been derived, which allow an acoustic simulation based on incompressible and compressible flow solutions. For the low Mach number flow simulation based on an incompressible approach the APE-2 formulation is most appropriate. The vortex sound source is the time derivative of the incompressible pressure $\partial P'/\partial t$. The APE-4 formulation for compressible flow simulations is not restricted to low Mach number problems. The vortex source term of the APE-4 system is the perturbation Lamb vector $(\boldsymbol{\omega} \times \boldsymbol{u})'$.

The error of the homogeneous APE system to predict convection effects in mean flows with vorticity has been tested against solutions of the linearized Euler equations for the sound field of a monopole in a sheared mean flow. The mean flow vorticity had only a small impact on the accuracy to predict convection effects. The sound generated by a spinning vortex pair showed a convincing agreement of the numerical solutions based on the APE-2 and APE-4 formulations and the analytical results based on a matched asymptotic expansion. Finally, a laminar flow over a cylinder at $M = 0.3$ and $Re = 200$ has been used to compare the results of a highly resolved unsteady CFD simulation with the findings of the hybrid approach. While the solution of the linearized Euler equations suffered from excessive artificial vorticity, the generation of undue vorticity could be successfully prevented using the acoustic perturbation equations. The APE systems yielded convincing results for the structure of the pressure contours and the decay of the pressure with increasing distance from the cylinder.

Acknowledgements

This work was supported by the Bundesministerium für Bildung, Wissenschaft, Forschung und Technologie (BMBF) under grant number 20A9702B and partially by the Deutsche Forschungsgemeinschaft (DFG) under grant number SCHR 309/15.

Appendix A

The two-dimensional linearized Euler equations given in Eqs. (1) and (2) can be expressed in wave number and frequency space by combined Fourier and Laplace transformation of the governing system of equations. For any scalar function $f(x,y,t)$ the Fourier transform of the spatial coordinates and the Laplace transformation of the time coordinate leads to the general form $\widetilde{f}(\alpha,\beta,\bar{\omega}) = \mathscr{T}(f(x,y,t))$, i.e.,

$$\widetilde{f}(\alpha,\beta,\bar{\omega}) = \frac{1}{(2\pi)^3}\int_0^\infty\!\!\int\!\!\int_{-\infty}^{\infty} f(x,y,t)\mathrm{e}^{-\mathrm{i}(\alpha x+\beta y-\bar{\omega}t)}\,\mathrm{d}x\,\mathrm{d}y\,\mathrm{d}t. \tag{A.1}$$

The wave numbers α and β are related to the spatial coordinates x and y and $\bar{\omega}$ is a complex quantity

$$\bar{\omega} = \omega + \mathrm{i}\sigma, \tag{A.2}$$

where the real part ω is the angular frequency and the imaginary part σ is a constant. The transformation has the properties that spatial derivatives are expressed in transformed space via

$$\mathscr{T}\left(\frac{\partial^n f}{\partial x^n}\right) = (\mathrm{i}\alpha)^n \widetilde{f}, \quad \mathscr{T}\left(\frac{\partial^n f}{\partial y^n}\right) = (\mathrm{i}\beta)^n \widetilde{f}. \tag{A.3}$$

The transform of the first time derivative obeys

$$\mathscr{T}\left(\frac{\partial f}{\partial t}\right) = -\mathrm{i}\bar{\omega}\widetilde{f} - \frac{1}{2\pi} f^*_{\text{initial}} \tag{A.4}$$

such that through the Laplace transformation initial values have to be considered. The quantity f^*_{initial} in Eq. (A.4) denotes the Fourier transform of $f(x,y,t)$ at time level $t = 0$

$$f^*_{\text{initial}}(\alpha,\beta) = \frac{1}{(2\pi)^2} \int\int_{-\infty}^{\infty} f(x,y,0)\mathrm{e}^{-\mathrm{i}(\alpha x+\beta y)}\,\mathrm{d}x\,\mathrm{d}y. \tag{A.5}$$

The inverse transformation of Eq. (A.1) is defined by

$$f(x,y,t) = \int\int_{-\infty}^{\infty} \int_{-\infty+\mathrm{i}\sigma}^{\infty+\mathrm{i}\sigma} \widetilde{f}(\alpha,\beta,\bar{\omega})\mathrm{e}^{\mathrm{i}(\alpha x+\beta y-\bar{\omega}t)}\,\mathrm{d}\bar{\omega}\,\mathrm{d}\beta\,\mathrm{d}\alpha, \tag{A.6}$$

where the constant σ in Eq. (A.2) is chosen such that the integration path of the inner integral is parallel to the real x-axis in the complex $\bar{\omega}$-plane above all poles of the integrand. Applying the transformation to each equation of the linearized Euler equations (1) yields the formal solution

$$\boldsymbol{A}\widetilde{\boldsymbol{U}} = \widetilde{\boldsymbol{G}}. \tag{A.7}$$

The quantity $\widetilde{\boldsymbol{U}} = (\widetilde{\rho}, \widetilde{u}, \widetilde{v}, \widetilde{p})^{\mathrm{T}}$ denotes the transform of the vector of the primitive variables and the matrix $\boldsymbol{A}$ follows from the flux vectors $\boldsymbol{E}$ and $\boldsymbol{F}$ by applying Eqs. (A.3) and (A.4), i.e., the terms are multiplied by the imaginary number i, and all initial conditions are shifted to the right-hand side to result in

$$\boldsymbol{A} = \begin{pmatrix} (\bar{\omega} - \alpha u_\infty) & -\rho_\infty \alpha & -\rho_\infty \beta & 0 \\ 0 & (\bar{\omega} - \alpha u_\infty) & 0 & -\alpha/\rho_\infty \\ 0 & 0 & (\bar{\omega} - \alpha u_\infty) & -\beta/\rho_\infty \\ 0 & -\gamma p_\infty \alpha & -\gamma p_\infty \beta & (\bar{\omega} - \alpha u_\infty) \end{pmatrix}. \tag{A.8}$$

The transform of the source vector is obtained analogously

$$\widetilde{\boldsymbol{G}} = \mathrm{i}\left(\widetilde{\boldsymbol{S}} + \frac{1}{2\pi}\boldsymbol{U}^*_{\text{initial}}\right), \tag{A.9}$$

where $\boldsymbol{U}^*_{\text{initial}}$ represents the initial values of the primitive variables at time level $t = 0$, which follow from Eq. (A.5). The eigenvalues λ_j and eigenvectors $\boldsymbol{x}_j$ of the matrix $\boldsymbol{A}$ are

$$\begin{aligned} \lambda_1 &= \lambda_2 = (\bar{\omega} - \alpha u_\infty), \\ \lambda_3 &= (\bar{\omega} - \alpha u_\infty) + c_\infty(\alpha^2 + \beta^2)^{1/2}, \\ \lambda_4 &= (\bar{\omega} - \alpha u_\infty) - c_\infty(\alpha^2 + \beta^2)^{1/2}, \end{aligned} \tag{A.10}$$

$$\boldsymbol{x}_1 = \begin{pmatrix} 1 \\ 0 \\ 0 \\ 0 \end{pmatrix}, \quad \boldsymbol{x}_2 = \begin{pmatrix} 0 \\ \beta \\ -\alpha \\ 0 \end{pmatrix}, \tag{A.11}$$

$$\boldsymbol{x}_3 = \begin{pmatrix} c_\infty^{-2} \\ \frac{-\alpha}{\rho_\infty c_\infty (\alpha^2+\beta^2)^{1/2}} \\ \frac{-\beta}{\rho_\infty c_\infty (\alpha^2+\beta^2)^{1/2}} \\ 1 \end{pmatrix}, \quad \boldsymbol{x}_4 = \begin{pmatrix} c_\infty^{-2} \\ \frac{\alpha}{\rho_\infty c_\infty (\alpha^2+\beta^2)^{1/2}} \\ \frac{\beta}{\rho_\infty c_\infty (\alpha^2+\beta^2)^{1/2}} \\ 1 \end{pmatrix}, \tag{A.12}$$

and $c_\infty = (\gamma p_\infty/\rho_\infty)^{1/2}$ denotes the sonic speed. The eigenvectors (A.11) and (A.12) are related to the different eigenmodes. The first two eigenvalues describe two convection modes. The eigenvector $\boldsymbol{x}_1$ is only nonzero in the first component. Therefore, this eigenvector is related to a convection mode of the density and can be identified as entropy mode. The second eigenvector describes velocity disturbances and is related to a vorticity mode. The eigenvectors $\boldsymbol{x}_3$ and $\boldsymbol{x}_4$ are related to acoustic modes. In general the transform of the vector of the primitive variables can be expressed as a linear combination of the eigenvectors, i.e.,

$$\widetilde{\boldsymbol{U}} = \frac{C_1}{\lambda_1}\boldsymbol{x}_1 + \frac{C_2}{\lambda_2}\boldsymbol{x}_2 + \frac{C_3}{\lambda_3}\boldsymbol{x}_3 + \frac{C_4}{\lambda_4}\boldsymbol{x}_4 = \boldsymbol{X}\boldsymbol{\Lambda}^{-1}\cdot\boldsymbol{C}, \tag{A.13}$$

where the columns of the matrix $\boldsymbol{X}$ are the eigenvectors $\boldsymbol{x}_j$. The components C_i of the vector $\boldsymbol{C}$ can be evaluated by inserting Eq. (A.13) into Eq. (A.7) and using $\boldsymbol{A} = \boldsymbol{X}\boldsymbol{\Lambda}\boldsymbol{X}^{-1}$

$$\boldsymbol{C} = \boldsymbol{X}^{-1}\widetilde{\boldsymbol{G}}. \tag{A.14}$$

The inverse eigenvector matrix for a parallel mean flow in the x-direction reads

$$\boldsymbol{X}^{-1} = \begin{pmatrix} 1 & 0 & 0 & -\frac{1}{c_\infty^2} \\ 0 & \frac{\beta}{\alpha^2+\beta^2} & -\frac{\alpha}{\alpha^2+\beta^2} & 0 \\ 0 & -\frac{1}{2}\frac{\rho_\infty c_\infty \alpha}{(\alpha^2+\beta^2)^{1/2}} & -\frac{1}{2}\frac{\rho_\infty c_\infty \beta}{(\alpha^2+\beta^2)^{1/2}} & \frac{1}{2} \\ 0 & \frac{1}{2}\frac{\rho_\infty c_\infty \alpha}{(\alpha^2+\beta^2)^{1/2}} & \frac{1}{2}\frac{\rho_\infty c_\infty \beta}{(\alpha^2+\beta^2)^{1/2}} & \frac{1}{2} \end{pmatrix}. \tag{A.15}$$

References

[1] S. Bergliaffa, K. Hibberd, M. Stone, M. Visser, Wave equation for sound in fluids with vorticity, LANL preprint cond-mat/0106255, 2001.

[2] B.-T. Chu, S. Kovásznay, Non-linear interactions in a viscous heat-conducting compressible gas, J. Fluid Mech. 3 (1958) 494–514.

[3] A.J. Cooper, N. Peake, Propagation of unsteady disturbances in a slowly varying duct with mean swirling flow, J. Fluid Mech. 445 (2001) 207–234.

[4] D. Crighton, Airframe noise, in: H. Hubbard (Ed.), Aeroacoustics of Flight Vehicles, 1991 (NASA TR 90-3052).

[5] J. Delfs, J. Yin, X. Li, Leading edge noise studies using CAA, Paper 99-1897, AIAA, 1999.

[6] T. Dong, C. Tam, N. Reddy, Direct numerical simulation of flap side edge noise, Paper 99-1803, AIAA, 1999.

[7] A. Dowling, J.F. Williams, M. Goldstein, Sound production in a moving stream, Phil. Trans. Roy. Soc. A 288 (1978) 321–349.

[8] J. Ekaterinaris, New formulation of Hardin–Pope equations for aeroacoustics, AIAA J. 37 (9) (1999) 1033–1039.

[9] R. Ewert, M. Meinke, W. Schröder, Computation of trailing edge noise via LES and acoustic perturbation equations, Paper 2002-2467, AIAA, 2002.

[10] R. Ewert, W. Schröder, M. Meinke, W. El-Askary, LES as a basis to determine sound emission, Paper 2002-0568, AIAA, 2002.
[11] J. Freund, Proposed inflow/outflow boundary condition for direct computation of aerodynamic sound, AIAA J. 35 (4) (1997) 740–742.
[12] M. Goldstein, Aeroacoustics, McGraw-Hill, New York, 1976.
[13] M. Goldstein, Unsteady vortical and entropic disturbances of potential flows round arbitrary obstacles, J. Fluid Mech. 891 (1978) 433–468.
[14] V. Golubev, H. Atassi, Acoustic-vorticity waves in swirling flows, J. Sound Vib. 209 (2) (1998) 203–222.
[15] H. Grogger, M. Lummer, T. Lauke, Simulating the interaction of a three-dimensional vortex with airfoils using CAA, Paper 2001-2137, AIAA, 2001.
[16] J. Hardin, D.S. Pope, An acoustic/viscous splitting technique for computational aeroacoustics, Theoret. Comput. Fluid Dynamics 6 (1994) 323–340.
[17] J. Hardin, D.S. Pope, Sound generation by flow over a two-dimensional cavity, AIAA J. 33 (6) (1995) 407–412.
[18] M. Howe, Acoustics of Fluid–Structure Interactions, Cambridge University Press, Cambridge, 1998.
[19] M. Howe, On the scattering of sound by a rectilinear vortex, J. Sound Vib. 227 (5) (1999) 1003–1017.
[20] M.S. Howe, Contributions to the theory of aerodynamic sound, with application to excess jet noise and the theory of the flute, J. Fluid Mech. 71 (4) (1975) 625–673.
[21] F.Q. Hu, M.Y. Hussaini, J.L. Manthey, Low-dissipation and low-dispersion Runge–Kutta schemes for computational acoustics, J. Comput. Phys. 124 (1996) 177–191.
[22] D. Lee, S. Koo, Numerical study of sound generation due to a spinning vortex pair, AIAA J. 33 (1) (1995) 20–26.
[23] S. Lele, Computational aeroacoustics, a review, Paper 97-0018, AIAA, 1997.
[24] M.J. Lighthill, On sound generated aerodynamically: I. General theory, Proc. R. Soc. London Ser. A 211 (1952) 564–587.
[25] G. Lilley, On the noise from jets, in: AGARD CP-131, 1974, pp. 13.1–13.12.
[26] E. Manoha, B. Troff, P. Sagaut, Trailing-edge noise prediction using large-eddy simulation and acoustic analogy, AIAA J. 38 (4) (2000) 575–583.
[27] W. Möhring, Modelling low mach number noise, in: E.-A. Müller (Ed.), Mechanics of Sound Generation in Flows, Springer, Berlin, 1979.
[28] W. Möhring, A well posed acoustic analogy based on a moving acoustic medium, in: P. Költzsch, N. Kalitzin (Eds.), Aeroacoustic Workshop, 1999.
[29] P. Morris, F. Farassat, Acoustic analogy and alternative theories for jet noise prediction, AIAA J. 40 (4) (2002) 671–680.
[30] E.-A. Müller, F. Obermeier, The spinning vorticies as a source of sound, in: AGARD CP-22, 1967, pp. 177–195.
[31] A. Pierce, Wave equation for sound in fluids with unsteady inhomogeneous flow, J. Acoust. Soc. Am. 87 (6) (1990) 2292–2299.
[32] D. Pope, A viscous/acoustic splitting technique for aeolian tone prediction, in: Second Computational Aeroacoustic (CAA) Workshop on Benchmark Problems, 1997 (NASA CP 3352).
[33] A. Powell, Theory of vortex sound, J. Acoust. Soc. Am. 36 (1) (1964) 177–195.
[34] H.S. Ribner, Perspectives on jet noise, Paper 81-0428, AIAA, 1981.
[35] W.Z. Shen, J.N. Sørensen, Aeroacoustic modelling of low-speed flows, Theoret. Comput. Fluid Dynamics 13 (1999) 271–289.
[36] W.Z. Shen, J.N. Sørensen, Comment on the aeroacoustic formulation of Hardin and Pope, AIAA J. 37 (1999) 141–143.
[37] S. Slimon, M. Soteriou, D. Davis, Computational aeroacoustics simulations using the expansion about incompressible flow approach, AIAA J. 37 (4) (1999) 409–416.
[38] C. Tam, Z. Dong, A study of the short wave components in computational acoustics, J. Comput. Acoust. 1 (1) (1993) 1–30.
[39] C. Tam, Z. Dong, Wall boundary condition for high-order finite-difference schemes in computational aeroacoustics, Theoret. Comput. Fluid Dynamics 6 (6) (1994) 303–322.
[40] C. Tam, J. Webb, Dispersion-relation-preserving finite difference schemes for computational acoustics, J. Comput. Phys. 107 (1993) 262–281.
[41] O. Vasilyev, A general class of commutative filters for LES in complex geometries, J. Comput. Phys. 146 (1998) 82–104.